AGU PUBLICATIONS

JGR

Journal of Geophysical Research: Earth Surface

RESEARCH ARTICLE

10.1002/2013JF002810

Key Points:

- Rivers and offshore plumes share a dynamic boundary condition at the river mouth
- Multiple floods produce transient river-bed adjustment and non-uniform flow
- Offshore plumes self-channelize by levee deposition and channel-bed scour

Correspondence to:
P. Chatanantavet,
Phairot.Chatanantavet@umontana.edu

Citation:
Chatanantavet, P., and M. P. Lamb (2014), Sediment transport and topographic evolution of a coupled river and river plume system: An experimental and numerical study, *J. Geophys. Res. Earth Surf.*, *119*, doi:10.1002/2013JF002810.

Received 27 MAR 2013
Accepted 28 APR 2014
Accepted article online 4 MAY 2014

Sediment transport and topographic evolution of a coupled river and river plume system: An experimental and numerical study

Phairot Chatanantavet[1] and Michael P. Lamb[1]

[1]Division of Geological and Planetary Sciences, California Institute of Technology, Pasadena, California, USA

Abstract Sediment transfer from rivers to the ocean is the fundamental driver of continental sedimentation with implications for carbon burial, land use dynamics, and unraveling global climate change and Earth history from sedimentary strata. Coastal rivers are dynamically coupled to their offshore plumes at the river mouth creating regions of nonuniform flow that can dictate patterns of erosion and deposition both onshore and offshore. However, there are limited experimental and modeling studies on sediment transport and morphodynamics of coupled river and river plume systems and their response to multiple flood events. To address this knowledge gap, we developed a quasi-2-D, morphodynamic numerical model and conducted exploratory flume experiments in a 7.5 m long flume where a 10 cm wide river channel was connected to a 76 cm wide "ocean basin." Both the numerical model and the flume results demonstrate that (1) during low-discharge flows, backwater hydrodynamics cause spatial-flow deceleration and deposition in the river channel and the offshore plume area, and (2) during high flows the water surface is drawn down to sea level, resulting in spatial-flow acceleration and bed scour. During high-discharge flows, we also found that the offshore river plume self-channelized owing to both levee formation and bed scour. Our study suggests that coastal rivers may be in a perpetual state of morphodynamic adjustment and highlights the need to link rivers and river plumes under a suite of flow discharges to accurately predict fluvio-deltaic morphodynamics and connectivity between fluvial sediment sources and marine sinks.

1. Introduction

Sediment transfer from rivers to the ocean is the fundamental driver of continental sedimentation with implications for carbon burial, land use management, reservoir architecture, and unraveling global climate change and Earth history from sedimentary strata [e.g., *Nittrouer*, 1999; *Blum and Tornqvist*, 2000; *Paola*, 2000; *Allison et al.*, 2010]. An important component of source-to-sink transfer is the river mouth where sediment from the fluvial system is transferred offshore. Much of the world's population lives near river mouths and deltas, where small imbalances in rates of sediment supply, subsidence, and sea level rise can heighten vulnerability to land loss and catastrophic inundation from storms, hurricanes, and tsunamis [*Tornqvist et al.*, 2007; *Blum and Roberts*, 2009; *Jerolmack*, 2009; *Syvitski et al.*, 2009; *Kim et al.*, 2009a; *Paola et al.*, 2011].

Rivers and offshore plumes are usually treated separately with a fixed boundary condition at the river mouth [*Bates*, 1953; *Wright*, 1977; *Nittrouer and Wright*, 1994; *Swenson et al.*, 2005; *Edmonds and Slingerland*, 2008; *Parker et al.*, 2008b]; however, river mouth hydrodynamics and sediment transport processes are affected by both fluvial and marine processes, thereby dynamically coupling the onshore and offshore systems. For example, the hydrodynamics of large coastal rivers with small channel-bed slopes are particularly sensitive to downstream boundary conditions owing to their small (subcritical) Froude numbers (i.e., $Fr < 1$, where $Fr \equiv U/\sqrt{gh}$, U is the cross-sectional average flow velocity, g is gravitational acceleration, and h is water depth). The Froude number in open-channel flow describes the speed of water flow relative to the speed of shallow water waves, waves that ultimately transmit boundary conditions upstream [e.g., *Chow*, 1959]. On the Mississippi River, USA, for example, $Fr \sim 0.2$ and changes in the water surface elevation at the river mouth (e.g., due to storm surge) can affect river flow velocities ~500 km upstream [e.g., *Nittrouer et al.*, 2012]. This zone of affected flow is referred to as *backwater* and is typified by spatially accelerating or decelerating flow resulting from a hydrodynamic boundary condition at the river mouth (Figure 1). Supercritical flows ($Fr > 1$) are not affected by downstream boundary conditions and consequently do not produce backwater because surface waves cannot propagate upstream.

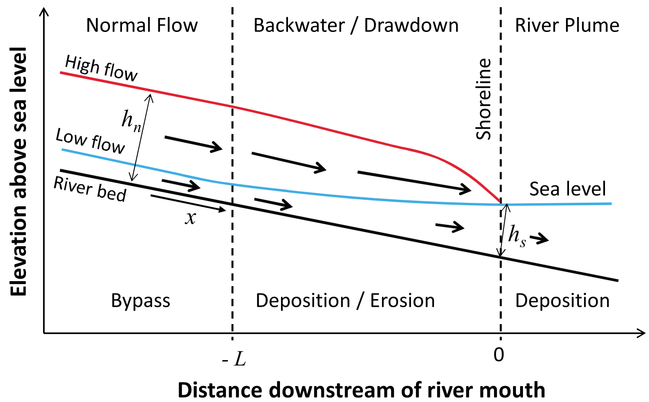

Figure 1. Schematic showing a river entering an ocean or lake with three zones: normal flow ($x < -L$), a transitional or backwater zone ($0 > x > -L$), and the offshore river plume ($x > 0$). At low flow (blue line), in the transitional zone there is spatial deceleration of flow where the water depth at shoreline is larger than the normal-flow depth upstream (i.e., M1 curve [e.g., *Chow*, 1959]), resulting in bed deposition. At high flow (red line), in the transitional zone there is spatial acceleration of flow where the water depth at shoreline is lower than the normal-flow depth upstream (i.e., M2 curve [e.g., *Chow*, 1959] or drawdown), resulting in bed erosion. In both cases, the water surface elevation at the river mouth is relatively insensitive to flow discharge due to lateral spreading of the offshore plume.

Although backwater hydrodynamics have been studied for more than a century [e.g., *Bresse*, 1860], their implications for sediment transport and morphodynamics have received comparatively little study. Following *Lane* [1957], *Lamb et al.* [2012], and *Nittrouer et al.* [2012] illustrated that during low-discharge events on the Mississippi River, the water depth at the river mouth (h_s) is greater than the normal (i.e., steady and uniform) flow depth (h_n) resulting in spatial deceleration of flow and deposition within the lower ~ 500 km of the river (Figure 1). In contrast, high-discharge events can produce spatial acceleration of flow, drawdown of the water surface, and riverbed scour within the backwater zone (Figure 1). These ideas are consistent with field surveys by *Nittrouer et al.* [2011], which show that a large portion of the final 165 km in the lower Mississippi River consists of substrate devoid of active alluvial cover. Bathymetric surveys on other river deltas such as Wax Lake, Louisiana, USA, also show scour upstream of river bifurcations [e.g., *Galler et al.*, 2003; *Shaw et al.*, 2013]. Using a morphodynamic model, *Chatanantavet et al.* [2012] showed how multiple flood discharges are needed to produce a persistent backwater zone, whereas under the common modeling assumption of constant water discharge, the riverbed tends to adjust so that normal flow eventually exists everywhere. Ultimately, nonuniform flow that manifests through multiple river floods may set locus of avulsion on deltas and therefore the characteristic size of many of the world's deltas [*Jerolmack and Swenson*, 2007; *Chatanantavet et al.*, 2012]. Backwater dynamics may also reduce river sinuosity, create regional-scale stratigraphic unconformities, and modulate magnitude-frequency relationships for source-to-sink sediment flux [*Lamb et al.*, 2012; *Nittrouer et al.*, 2012; *Blum et al.*, 2013].

Erosion and deposition in coastal rivers and deltas are typically thought to occur due to sea level rise, subsidence, or changes in the balance between sediment supply and the sediment transport capacity of the feeder river [e.g., *Paola*, 2000]. The latter effect is well known in fluvial geomorphology and results in a change in equilibrium riverbed slope [e.g., *Lane*, 1955]. Nonuniform flow forced by river mouth boundary conditions within backwater zones provides an important additional mechanism for riverbed erosion and deposition in coastal rivers, a mechanism that is rarely included in models. For example, most numerical models either neglect the backwater zone completely [e.g., *Flemings and Jordan*, 1989; *Paola et al.*, 1992; *Swenson et al.*, 2005] or assume a single characteristic discharge which prevents the backwater zone from being dynamic [e.g., *Snow and Slingerland*, 1987; *Hotchkiss and Parker*, 1991; *Slingerland et al.*, 1994; *Parker et al.*, 2008a]. Most flume experiments also use a single characteristic discharge or relatively steep bed slopes (with supercritical Froude numbers) in comparison to natural rivers, which minimizes or eliminates the backwater zone [e.g., *Muto*, 2001; *Sheets et al.*, 2002; *Swenson and Muto*, 2007; *Parker et al.*, 2008b].

Offshore, it is well known that the fluid dynamics and sedimentation patterns of river plumes are also strongly affected by the boundary conditions at the river mouth [e.g., *Bates*, 1953; *Rajaratnam*, 1976; *Wright*, 1977; *Nittrouer and Wright*, 1994; *Geyer et al.*, 2004; *Falcini and Jerolmack*, 2010]. For example, in the near-field river plumes undergo lateral expansion [*Wright and Coleman*, 1971; *Hetland and MacDonald*, 2008] often increasing by an order of magnitude in width over the first few kilometers, which is set in part by river width-to-depth ratio and flow velocity at the river mouth [*Wright and Coleman*, 1971; *Wright*, 1977; *Hetland*, 2010]. The initial buoyancy of the plume is controlled by mixing with ambient water in the estuary [*Nash et al.*, 2009] and the plume liftoff region [*MacDonald and Geyer*, 2004], and the suspended sediment concentration of the plume, which controls whether plumes are buoyant at low concentrations (i.e., hypopycnal plumes) or plunge to form turbidity currents at high concentrations (i.e., hyperpycnal plumes) [*Bates*, 1953; *Wright et al.*, 1990; *Nittrouer and Wright*, 1994; *Mulder et al.*, 2003; *Geyer et al.*, 2004; *Lamb and Mohrig*, 2009; *Lamb et al.*, 2010].

River plumes interact with evolving bed topography, which in cases can lead to the formation of levees and mouth bars [e.g., *Edmonds and Slingerland*, 2007; *Rowland et al.*, 2009; *Edmonds et al.*, 2010; *Edmonds and Slingerland*, 2010; *Rowland et al.*, 2010; *Mariotti et al.*, 2013; *Canestrelli et al.*, 2014; *Falcini et al.*, 2014], yet the process of plume self-channelization is not well understood. Most previous experimental work on sediment-laden plumes and deltas has emphasized the role of aggradational levees in confining river plumes. However, these studies typically have neglected an extensive, alluvial feeder river channel thereby imposing the relative balance of sediment and water fluxes at the river mouth [e.g., *Hoyal and Sheets*, 2009; *Rowland et al.*, 2010; *Kim et al.*, 2010; *Powell et al.*, 2012]. In contrast, other experiments have produced channelization by bed scour (rather than levee aggradation), but only under the case of a clear water, planar jet that lacks sediment feed [e.g., *Rajaratnam and Berry*, 1977; *Rajaratnam*, 1981; *Rajaratnam and Macdougall*, 1983; *Mason and Arumugam*, 1985; *Hogg et al.*, 1997; *Dey and Sarkar*, 2006; *Faruque et al.*, 2006; *Sui et al.*, 2008]; it is unclear if such bed scour would occur from a river plume fed by an alluvial river transporting sediment at its capacity. *Rowland et al.* [2010] used a sediment-laden planar jet to investigate self-channelization, but over a nonerodible bed and without an alluvial feeder channel. *Rowland* et al. also emphasized the need for future work to investigate the effect of repeated flood events on subaqueous levee formation.

Despite important advances in previous work, there are fundamental unknowns about the morphodynamics of deltaic rivers and river plumes: How does nonuniform flow, arising over multiple flood events, influence sediment transport in the lowermost reaches of rivers? How do backwater-induced changes in sediment transport affect deltaic sedimentation and offshore river plume dynamics? Recent studies have addressed these questions in part, but there is a dearth of experimental data on the morphodynamics of coupled river and river plume systems with subcritical flow ($Fr < 1$) subject to multiple flood events. Herein, we report on laboratory experiments and numerical modeling designed to address this gap. First, we present the numerical model formulation. The experimental setup and methods are introduced second. Third, results from the flume experiments and the numerical model are presented. Finally, we discuss the implications for the persistence of backwater zones in natural deltaic rivers, the timescales of riverbed adjustment, and the mechanisms of river plume self-channelization.

2. Numerical Model Development

The numerical model used herein is similar to that presented in *Chatanantavet et al.* [2012] which was applied to the case of the Mississippi River. The model should apply to both field and laboratory scales allowing a means to upscale results from the laboratory experiments to the field. At laboratory scale, however, a moving-boundary technique is needed during low-flow events to accurately model the delta front [*Hotchkiss and Parker*, 1991]. Such moving-boundary techniques are well established for delta fronts and we follow the formulation of *Parker* [2004], which is not repeated here. The other parts of the model are briefly reviewed and the reader is referred to *Chatanantavet et al.* [2012] and *Lamb et al.* [2012] for more detail.

Conservation of fluid mass and momentum of the depth-averaged and width-averaged, 1-D spatially varied flow in the streamwise (x) direction [e.g., *Chow*, 1959] can be written as

$$\frac{\mathrm{d}(Uhw)}{\mathrm{d}x} = 0 \tag{1}$$

$$U\frac{\mathrm{d}U}{\mathrm{d}x} = -g\frac{\mathrm{d}h}{\mathrm{d}x} + gS - C_f\frac{U^2}{h} \tag{2}$$

where w is channel width, x is longitudinal distance downstream of river mouth, S is bed slope, and C_f is bed friction coefficient. The combination of equations (1) and (2) leads to a standard formulation of the backwater equation for spatially varied flow [*Chow*, 1959],

$$\frac{\mathrm{d}h}{\mathrm{d}x} = \frac{S + Fr^2\left(\frac{h\mathrm{d}w}{w\mathrm{d}x} - C_f\right)}{1 - Fr^2} \tag{3}$$

Offshore, river plumes tend to spread laterally and sometimes vertically due to loss of river channel confinement, resulting in offshore deposition and a water surface elevation at the river mouth that is relatively insensitive to changes in river discharge as compared to farther upstream [e.g., *Rajaratnam*, 1976; *Wright*, 1977; *Rowland et al.*, 2009; *Schiller and Kourafalou*, 2010]. The simplest way to incorporate the effect of lateral plume spreading would be to force the water surface elevation at the river mouth to be at sea level through use of a boundary condition at $x = 0$ in equation (3) [e.g., *Parker et al*., 2008a; *Karadogan et al*., 2009]. We have found, however, that forcing the water surface to sea level at $x = 0$ is too restrictive and can produce a drawdown effect that is greater than observed [*Lamb et al*., 2012]. To allow for some variation of the water surface elevation at the river mouth, we instead treat the offshore plume as a depth-averaged, steady, homopycnal current, where momentum is balanced in 1-D between a hydrostatic pressure gradient and drag along the bed (i.e., equation (3)). Following *Lamb et al*. [2012], we neglect drag and entrainment along the lateral margins of the plume and represent lateral spreading of the plume geometrically by assigning a set spreading angle (θ) beyond the shoreline ($x > 0$). Thus, in equation (3), the average width of the plume beyond the shoreline (i.e., $x > 0$) is calculated from $\frac{dw}{dx} = 2\tan\theta$ where θ is the spreading angle of the plume relative to the center streamline [e.g., *Wright and Coleman*, 1971; *Rajaratnam*, 1976].

We use *Wong and Parker*'s [2006] relationship for calculating the transport capacity of bed load sediment (Q_s) since it is the major transport mode in our experiments, written as

$$Q_S = 3.97\rho_S w\left(RgD_{50}^3\right)^{1/2}\left(\tau^* - \tau_C^*\right)^{3/2} \tag{4}$$

where R is the submerged specific density of the sediment ($R = \rho_s/\rho - 1$, ρ_s is density of sediment and ρ is density of water), D_{50} is the median grain size, $\tau_* = u_*^2/RgD_{50}$ is the Shields stress, $u_* = \sqrt{C_f U^2}$ is the shear velocity, and $\tau_c^* = 0.0495$ is the critical Shields stress. We assume that sediment transport is at capacity everywhere (i.e., no sediment supply limitation). The evolution of the bed by continuity of sediment then can be written as

$$\rho_s\left(1 - \lambda_p\right)\left(\frac{\partial\eta}{\partial t}\right) = -\frac{1}{w_d}\frac{\partial Q_s}{\partial x} \tag{5}$$

where λ_p is bed porosity, η is bed elevation, t is time, and w_d is the width of the depositional zone. In the river section ($x < 0$), the width of the depositional zone is equivalent to the channel width (i.e., $w_d = w$). The offshore depositional zone, however, can span a much larger area than the width of the river plume itself due to lateral translation of the plume. To account for this effect using our quasi-2-D framework, we follow previous work [e.g., *Parker and Sequeiros*, 2006; *Kim et al*., 2009b] and set the effective width of the offshore (i.e., $x > 0$) depositional zone to $w_d = w_o + 2x\tan\theta_d$, where w_o is the river channel width and θ_d is the deposit spreading angle relative to the centerline. Greater spreading angles result in slower delta vertical aggradation.

Equations (3)–(5) represent the quasi-2-D river plume morphodynamic model, which links hydrodynamics, sediment transport, and bed morphology and simulates the interactions among them. We solved the governing equations using finite difference approximations (first-order in time and second-order in space). Initially, the bed elevation, bed slope, channel width, and water discharge are specified everywhere along the flow path. The water level in the basin is fixed at sea level very far downstream of the region of interest ($x >> 0$), which allows a dynamic water surface elevation at the river mouth. The calculation for flow depth proceeds in an upstream direction from this boundary condition. Due to depth and width averaging, the model cannot produce true 2-D or 3-D effects that are apparent in experiments (e.g., levees), but it serves as a useful comparison to the experiments in 1-D along the flume centerline.

3. Experimental Setup

The experiments were conducted in the Earth Surface Dynamics Laboratory at the California Institute of Technology. The experiments were carried out using freshwater in a flume that is 4.5 m long, 0.6 m deep, and 0.1 m wide in the river section and 2.5 m long, 0.8 m deep, and 0.75 m wide in the "oceanic" basin portion (Figure 2). There was no density contrast between the river flow and the ocean basin in our experiments because previous work has shown that deltaic channels form only when there is frictional coupling between the flow and the bed [e.g., *Rowland et al*., 2010], which may occur in nature either because the plume and basin are of equal density (i.e., homopycnal) [e.g., *Rowland et al*., 2009] or because the plume has not reached sufficient depth to lift off or plunge (i.e., the "depth-limited plume" of *Lamb et al*. [2010]). The latter is likely the case for many rivers during flood where salt-water intrusions are pushed seaward [e.g., *Wright and Coleman*, 1974] and the depth required for buoyant liftoff is large [e.g., *Hetland and MacDonald*, 2008].

The water level in the basin section was fixed at the same level for different experiments using adjustable stand pipes at the end of the flume. Water discharge was measured using a magnetic flow meter mounted in line with the water supply piping. Sediment was fed through an auger-type sediment feeder at the upstream

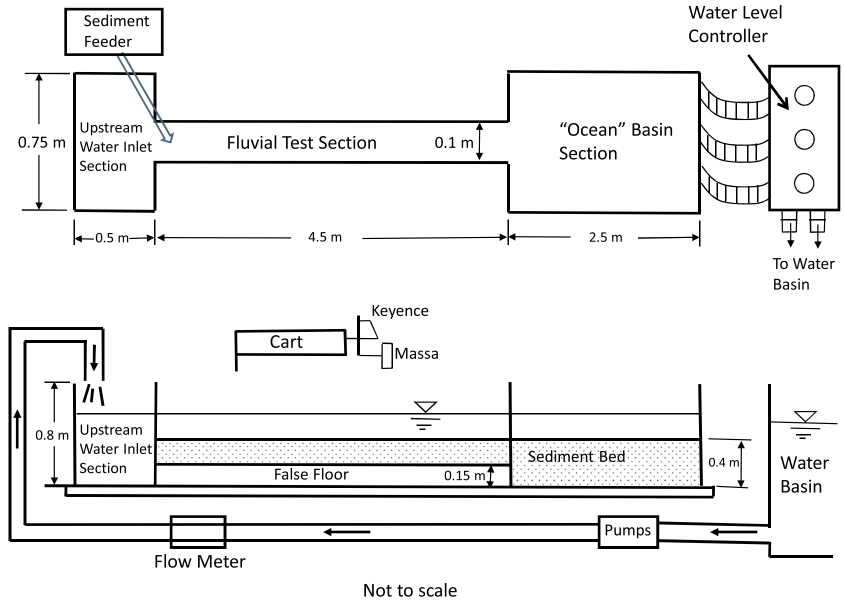

Figure 2. The experimental flume at Caltech used in this study to investigate river and river plume morphodynamics. (top) Top view and (bottom) side view. Flow is from left to right.

end. All experiments were conducted with uniform crushed walnut shells ($D = 0.7$ mm) for predominantly bed load sediment with some suspension at high-flow conditions. The walnut shells have a submerged specific density (R) of 0.3 ± 0.1, which was desirable for maintaining subcritical flows ($Fr < 1$). The Rouse number (P) was between 1 and 4.7 (Table 1) and calculated using $P = v_s/(\kappa\ u_*)$ where v_s is particle fall velocity in still water (32 mm/s), and κ is von Karman's constant of 0.41. Bed load is predominant when $P > 2.5$, and suspended load is predominant when $P < 1.0$ [*Bagnold*, 1956]. All of our experiments fall within the regime of intermittent suspension ($P < 6.1$ for large particle Reynolds numbers) found by *Rowland et al.* [2010] to be necessary for the formation of subaqueous levees [see also *Mariotti et al.*, 2013].

During the experiments the bed and water surface elevations were measured using a laser (Keyence CA-U2) and an ultrasonic distance meter (Massa), respectively. The instruments were mounted to a nonmotorized 3-D positioning instrument cart with submillimeter positioning accuracy. Bed topography was surveyed to

Table 1. Experimental Runs With Measured or Given Parameters

	Experiment 1 Low-Flow (M1) Equilibrium	Experiment 2 High-Flow (M2) Equilibrium	Experiment 3 Low-Flow Transient	Experiment 4 High-Flow Transient
Flow discharge, Q_w (l/s)	1.5	3.4	1.5	3.4
Sediment feed, Q_s (g/s)	1.1	1.9	1.1 (see Figure 6)	8.8 → 6.0
Run time, t (hrs)	10.5	7.25	21.5	1.72
In-channel water depth, h (cm)	6.4 ± 0.4	12.3 ± 0.8	12.3 ± 0.8 → 6.4 ± 0.4	6.4 ± 0.4 → 9.5 ± 0.7
In-channel water surface slope, S	0.0015	0.0015	0 → 0.0015	0.0044 → 0.0028
In-channel flow velocity, U (m/s)	0.23 ± 0.01	0.27 ± 0.02	0.13 ± 0.01 → 0.23 ± 0.02	0.51 ± 0.04 → 0.36 ± 0.06
In-channel Froude number, Fr	0.28 ± 0.02	0.24 ± 0.02	0.12 ± 0.01 → 0.29 ± 0.04	0.63 ± 0.07 → 0.40 ± 0.09
Reynolds number	14,720	33,210	15,990 → 14,720	32,640 → 34,200
Rouse number[a], P	2.7	1.9	4.7 → 2.7	1.0 → 1.4
Friction coefficient, C_f	0.017	0.024	0.017	0.024
Measured plume spreading angle, θ (degree)[b]	5.7 → 18.0 [18.0]	5.7 → 10.2 [10.2]	13.2 → 15.5 [13.2]	7.7 → 10.0 [7.7]
Measured sediment-deposit spreading angle, θ_d (degree)[b]	5.7 → 18.0 [34.0]	5.7 → 34.0 [25.0]	12.5 → 18.4 [34.0]	7.7 → 34.0 [25.0]

[a]Rouse number is defined as $P = v_s/u_*$ where v_s is particle fall velocity in still water, and κ is Karman constant = 0.41. Bed load is predominant when $P > 2.5$, and suspended load is predominant when $P < 1.0$. Between these thresholds, there is some suspended load [*Bagnold*, 1956].
[b]These spreading angles were measured in the flume. The values in [ ] were selected and used in the numerical modeling, in which they were assumed to be constant for each run.

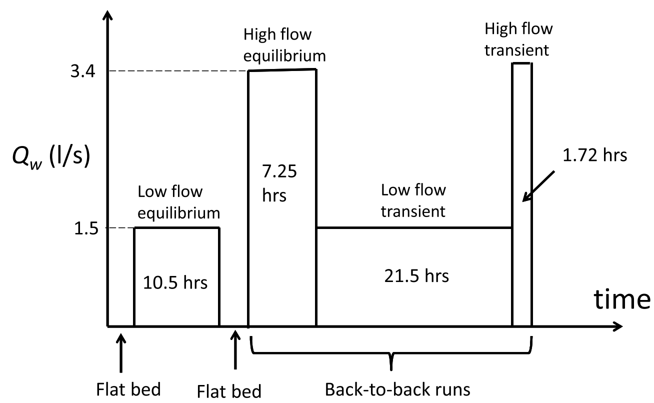

Figure 3. Experimental plan showing the low-flow (M1) and high-flow (M2) discharge (Q_w) with time. The equilibrium experiments started with a flat bed. The low-flow condition was run for 10.5 h to equilibrium where the bed morphology no longer significantly changed. Then, a flat bed was imposed again for the high-flow equilibrium run for 7.25 h. The final high-flow bed topography was used as the initial condition for the low-flow transient run that lasted for 21.5 h. The final bed topography from the low-flow transient case was used as the initial condition for the high-flow transient run that lasted for 1.72 h. Sediment supply was changed commensurate with water discharge to maintain a constant equilibrium bed slope under normal-flow conditions.

capture dominant breaks in slope at a horizontal spatial resolution of about 1 to 5 cm, and these were repeated every 0.5 to 2 h during an experiment. The experiment was stopped (no water flow) and the bed was submerged during bed topographic surveys, and the laser was emitted through the flat water surface. Measurements of submerged objects of known elevation and water depth provided the index-of-refraction correction used to convert obtained data to actual depths and elevations. Water surface elevations reported are the mean of measurements recorded over 60 s and sampled at 20 Hz.

During the experiments, dye pulses were injected into the water flow at the upstream end of the flume and recorded using an overhead video camera (40 frames/s) to calculate flow velocity of the offshore plume. The plume front was traced by eye on successive video frames separated by 0.082 s with a point spacing of ~ 3–10 mm. An algorithm was developed and used to calculate the velocity between two traced plume front profiles separated by some amount of time. At each measured point along the first plume-front profile, the algorithm calculates the local slope of the plume front from the neighboring two nodes, looks perpendicular to this slope, and uses linear interpolation to locate the intersection with the second plume front profile (set to be 0.4 s after the first-front profile to allow for some temporal averaging). Velocity for this node is then the perpendicular distance between the two front profiles divided by the time interval separating the two fronts. The resulting velocity field was noisy in cases due to the assumption that flow velocity was moving perpendicular to the front and due to turbulence and mixing along the boundaries of the front [e.g., *Mariotti et al.*, 2013]. To average over this variability and owing to the larger velocity gradients in the cross-stream direction, we used a moving average filter with a 40 cm windowing length in the streamwise direction and a 3 cm windowing length in the cross-stream direction. Depth-averaged flow velocity in the river channel section was calculated from mass balance using equation (1). The images of dye pulses were also used to measure the spreading angles of the plumes.

In order to test the effect of variable discharges on the coupled river and river plume system, we used two discharge events designed to produce backwater hydrodynamics and deposition for the low-flow event (i.e., M1 regime) [e.g., *Chow*, 1959], and drawdown hydrodynamics and scour at the high-flow event (i.e., M2 regime) [e.g., *Chow*, 1959] (Figure 1 and Table 1). Using the numerical model as a guide, the experimental water and sediment supply was set so that both discharge events created the equivalent equilibrium bed slope for normal-flow conditions in which sediment transport was at capacity (i.e., equation (4)). This is an important point because an imbalance between sediment supply and sediment transport capacity can produce erosion or deposition that results in adjustment of the equilibrium riverbed slope [e.g., *Lane*, 1955]. Our goal is to isolate erosion and deposition due to backwater dynamics alone. In addition to achieving the same equilibrium bed slope, the water and sediment flux values were chosen so that the two experiments produced subcritical flow and measurable changes in flow depth between the two cases.

Four experiments were completed (Table 1). The first experiment was designed to run the low-flow event (M1; flow discharge $Q_w = 1.5$ l/s, $Q_s = 1.1$ g/s, using equation (4) for transport capacity) to a state that approached topographic equilibrium, starting from a flat bed graded to about one normal-flow depth below sea level to shorten the time to equilibrium (Figure 3). The second experiment was the same as the first experiment but for the high discharge (M2; $Q_w = 3.4$ l/s, $Q_s = 1.9$ g/s). These two experiments are referred to as equilibrium runs.

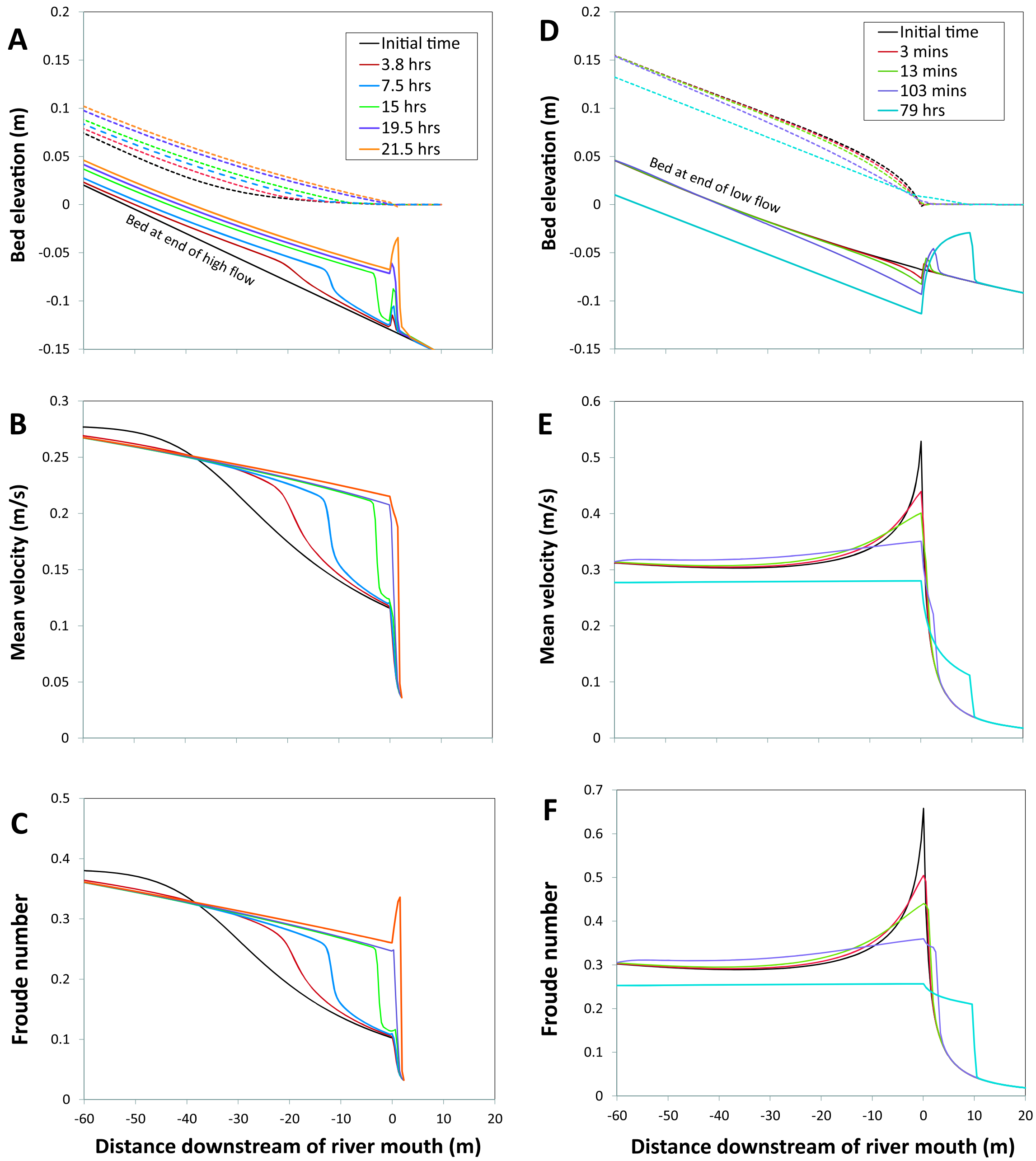

Figure 4. Numerical model results for (a–c) low-flow transient run, and (d–f) high-flow transient run. The plots include bed (solid lines) and water surface (dashed lines) elevations as shown in Figures 4a and 4d, mean flow velocity as shown in Figures 4b and 4e, and Froude number as shown in Figures 4c and 4f. Numerical model used the sediment-deposit and plume spreading angles measured in the experiments (Table 1).

For the third experiment, the low-flow event (same as in Experiment 1) was run over the final bed topography from Experiment 2 in order to observe the transient adjustment of the bed from a high-discharge flow to a low-discharge flow. Likewise, the fourth experiment was for a high-discharge event using the final bed from Experiment 3 as an initial condition to observe the transient adjustment of the bed from a low-discharge flow to a high-discharge flow. The latter two experiments will be referred to as transient runs. All experiments produced bed forms that affected the bed friction. A bed friction coefficient (C_f) was measured using $C_f = \frac{ghS}{U^2}$ under near normal-flow conditions from Experiments 1 and 2. These in channel (i.e., $x < 0$) measured C_f values of 0.017 and 0.024 for low- and high-discharge equilibrium runs, respectively, were used throughout the numerical modeling. We also assume that these values of C_f are valid for the offshore portions of flow.

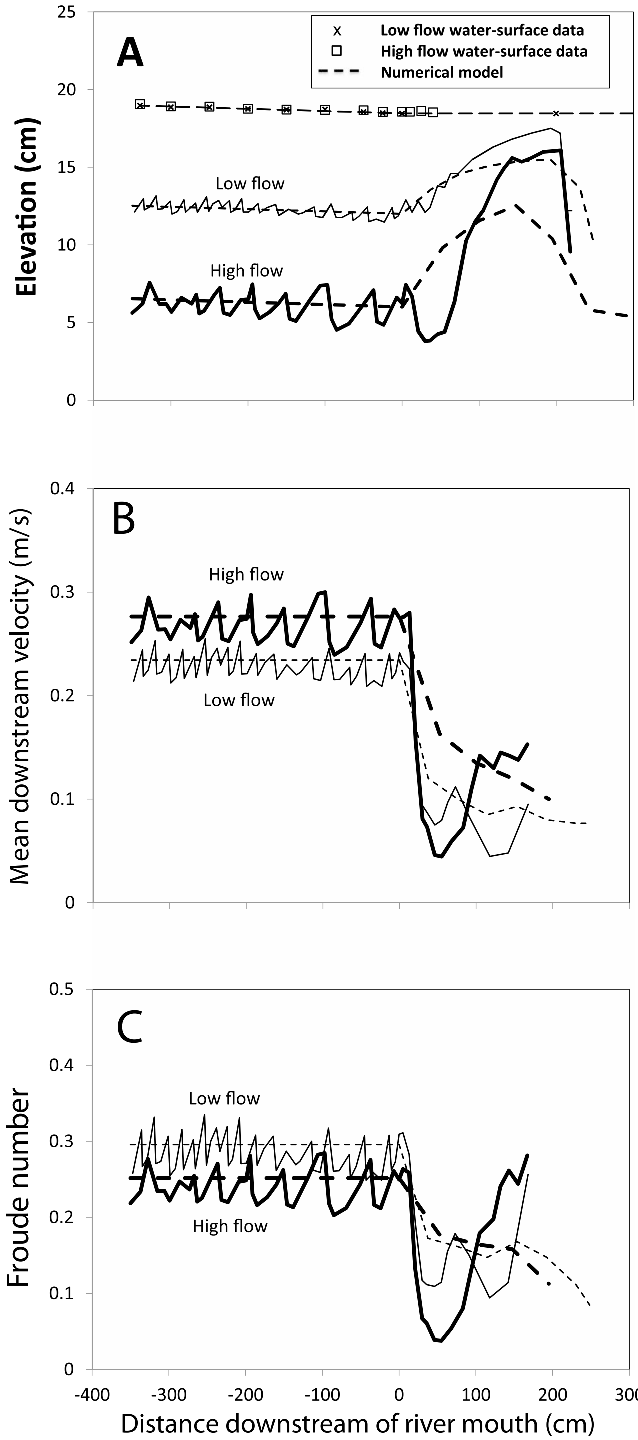

Figure 5. Experimental results along the flume centerline from the equilibrium runs for low-flow and high-flow conditions (Experiments 1 and 2) showing (a) bed and water surface elevations, (b) average flow velocity, and (c) Froude number. Dashed lines are from the numerical model and solid lines are the flume results. Flow is from left to right. The vertical axis is referenced to the flume bottom.

The experiments were not designed to simulate the entire backwater zone. This is in part because incorporating the entire backwater zone while maintaining subcritical Froude numbers and measurable water depths requires an experimental facility tens to hundreds of meters in length [e.g., *Hotchkiss and Parker*, 1991]. The numerical modeling results (discussed in section 4) indicate that the backwater effects in our experiments would have manifested over tens of meters had our experimental facility been longer. Thus, the experiments simulated the downstream ~10% of the backwater zone, as well as the offshore zone. Because downstream boundary conditions control the hydrodynamics in backwater zones, the absent upstream portion of the backwater zone should not affect the experimental results as long as the pacing of sediment feed at the upstream end of the flume is adjusted properly to account for transient bed adjustment. To accomplish this, the transient experiments used a time-dependent sediment feed rate to simulate morphodynamic changes in the portion of the backwater zone that extended beyond the length of our flume (discussed in detail in section 5.2).

4. Numerical Modeling Results

The numerical model developed in section 2 was run with the same input parameters used in the flume experiments (Table 1), namely, bed porosity = 0.49 (measured), plume spreading angles of 7.7 to 18° (measured from the experiments), sediment-deposit spreading angles of 25 to 34° (measured from the experiments), as well as a time step $\Delta t = 3.2$ s, and a grid spacing of $\Delta x = 0.5$ m. The fluvial channel length was set to 75 m and the basin length was set to 20 m in order to fully capture the nonuniform flow dynamics outside of the length-constraints of the experimental facility. Sediment supply at the upstream end of the model domain was set equal to the transport capacity under normal-flow conditions for the imposed water discharge, so that both high- and low-flow cases had the same final equilibrium bed slope. Therefore, like the experiments, any fluvial erosion or deposition observed in the simulations is due to nonuniform flow forced by boundary effects at the river mouth and the offshore plume.

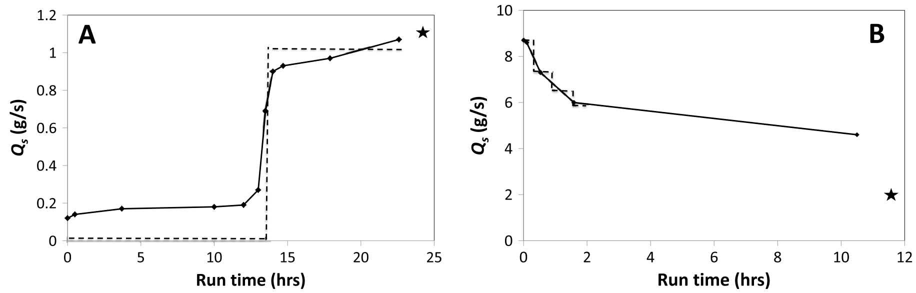

Figure 6. Numerical model output of sediment flux (Q_s) at $x = -4.5$ m as a function of time for A) Experiment 3 (low-flow transient run) and B) Experiment 4 (high-flow transient run). The dashed lines show the discretization of sediment feed rate that was used in the flume experiments. Experiment 4 was only run until $t = 1.72$ h. The stars indicate the sediment supply from the equilibrium experiments.

The first numerical experiment started with an equilibrium bed topography for the high-flow condition, and subjected it to the low-flow discharge ($Q_w = 1.5$ l/s) and corresponding sediment supply ($Q_s = 1.1$ g/s) set for the low-flow (M1) case (Table 1). At the beginning of the simulation, the water depth at the shoreline was greater than the normal depth for low flow, resulting in a concave upward water surface profile (Figure 4a), spatial deceleration of flow (Figure 4b), and highly subcritical flow (Figure 4c). The bed adjusted through a downstream-propagating wedge of sediment, and the rate of deposition was greatest just offshore of the river mouth where the offshore plume spreads resulting in a delta (Figure 4a). After 21.5 h, the water surface and bed slopes were nearly constant and equivalent, largely eliminating nonuniform flow and the associated divergences in sediment flux. The slight concavity in the bed profile that remained was a result of deposition forced by the aggrading and prograding offshore delta.

The second numerical experiment started with the equilibrium bed topography from the low-flow experiment and subjected it to the high-flow discharge ($Q_w = 3.4$ l/s) and corresponding sediment supply ($Q_s = 1.9$ g/s) for the high-flow event (Table 1). Spreading of the offshore plume rendered the water surface at the river mouth nearly fixed at sea level, which choked the high-discharge flow through a narrow cross section at the river mouth. Within minutes, the bed rapidly scoured just upstream of the river mouth, forced by water surface drawdown (Figure 4d) and spatial-flow acceleration (Figure 4e). Note the Froude number was still subcritical ($Fr < 0.65$) during this transient phase of scour (Figure 4f). Over time, the wave of erosion migrated upstream until a new equilibrium depth was established. The offshore ($x > 0$) delta also built over time due to decelerating flow caused by lateral spreading of the river plume. In the next section, we test these ideas using flume experiments designed to examine the region $-4.5 < x < 2.5$ m (Figure 4).

5. Experimental Results

5.1. Equilibrium Experiments

Experiments 1 and 2 were run with the initial flat-bed topography set everywhere to be approximately one normal depth below sea level (i.e., ~ 6 cm and ~ 12 cm for Experiments 1 and 2, respectively). After Experiment 1 was completed, the bed was regraded flat before running Experiment 2. For the low-flow case ($Q_w = 1.5$ l/s), the experiment was run for a total of 10.5 h, which was sufficiently long that bed topographic change was minor at the end of the experiment, except at the delta front in the basin. Likewise, for Experiment 2, the initial bed was flat, and the high-flow case ($Q_w = 3.4$ l/s) was run for a total of 7.25 h. For Experiments 1 and 2, measurements were taken only at the end of the experiments, when quasi-equilibrium conditions were reached and normal flow existed everywhere in the fluvial channel ($x < 0$). The results for these two experiments are shown in Figure 5 along with the corresponding numerical model results (section 4).

Experimental results show that the high- and low-flow cases had nearly identical final bed slopes and water surface slopes of 0.0015 in the river section ($x < 0$; Figure 5a) by design. Centimeter-scale roughness in the bed profiles was due to bed forms; larger bed forms in the high-flow case resulted in a larger observed friction coefficient (Table 1). The equilibrium flow depth for the high-flow case was about 12.3 cm, which was greater than the low-flow case of 6.4 cm. Depth-averaged flow velocities were 0.23 and 0.28 m/s in the river section for the low-and high-flow cases, respectively, with the centerline velocity of the plume ($x > 0$)

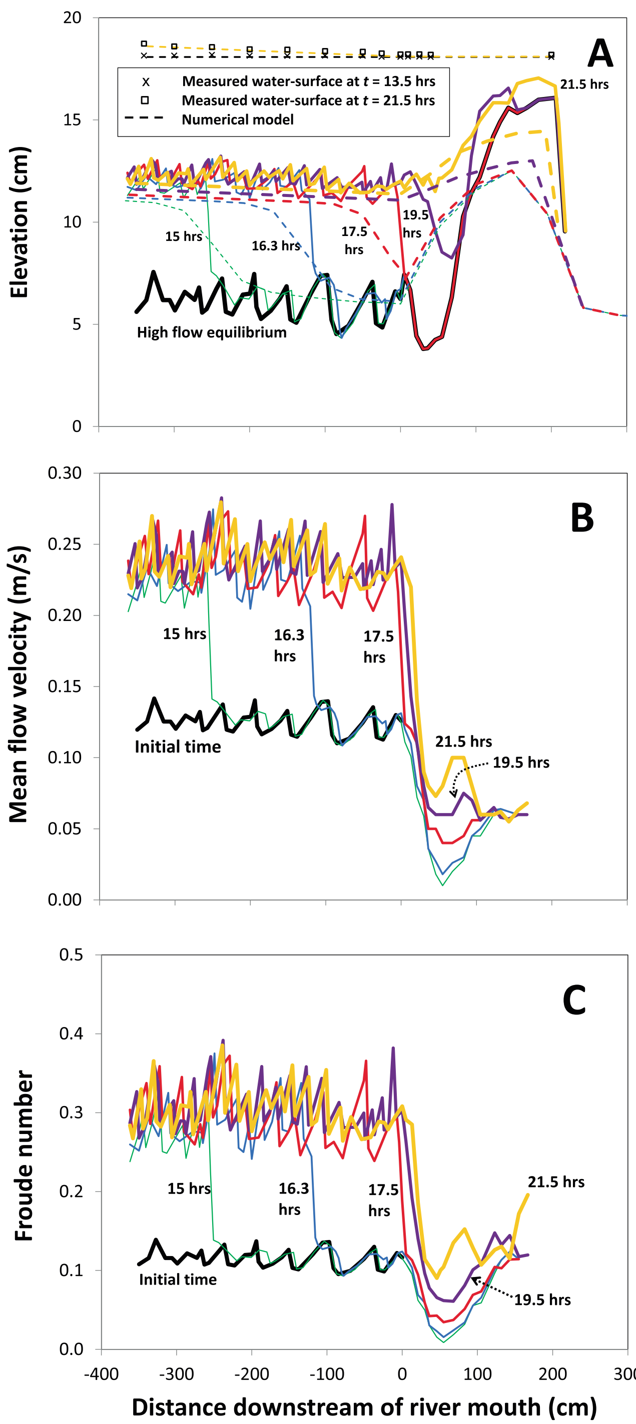

Figure 7. Experimental results from Experiment 3 (low-flow transient; solid lines) starting from high-flow equilibrium conditions (black lines) for (a) bed and water surface elevations, (b) mean flow velocity, and (c) Froude number. Dashed lines are from the numerical model. Flow is from left to right. The vertical axis is referenced to the flume bottom.

decreasing rapidly with distance offshore (Figure 5b) due to strong lateral spreading of the flow. The flow accelerated again in the most distal part of the experiment due to shallow flow depths caused by delta aggradation. This rapid spatial decrease in plume velocity within $0 < x < 60$ cm is coincident with rapid rates of deposition in the delta region (Figure 5a). However, for the high-flow case, we observed a region ($0 < x < 60$ cm) of bed scour ~ 3 cm deep relative to the bed upstream (Figure 5a) and ~12 cm deep relative to the lateral deposits, despite the apparent spatial deceleration of flow in this region. The Froude numbers for both events were similar and subcritical (Figure 5c). The Rouse numbers were calculated to be 2.7 and 1.9 for the low-flow and high-flow equilibrium runs, respectively, indicating that the low-flow case was predominantly in the bed load regime, and the high-flow case had some sediment suspended, consistent with our visual observations.

The numerical model reproduces the observed bed and water surface topography in the river section ($x < 0$) but underpredicts the peak bed elevation in the offshore region for both cases and does not predict the region of scour observed directly offshore of the river mouth for the high-flow event (Figure 5a). These inconsistencies between the model and the observations are likely a result of full 2-D and 3-D morphodynamics, which are not represented in the model, explored further in section 5.3.

5.2. Transient Experiments

The transient experiments were designed to examine how the bed adjusts from the high-flow event to the low-flow event (Experiment 3) and from the low-flow event to the high-flow event (Experiment 4) (Table 1). These experiments are similar to Experiments 1 and 2, but here the initial bed condition was not flat but rather was the inherited bed topography from the previous experiment, similar to the numerical experiments in section 4. Another difference in these experiments is that, owing to the initial bed topography being out of morphodynamic equilibrium with the flow conditions, we used a temporally varying sediment feed at the upstream end of the flume to simulate the effect of aggradation in the upstream part of the backwater zone that was not captured within the length of our

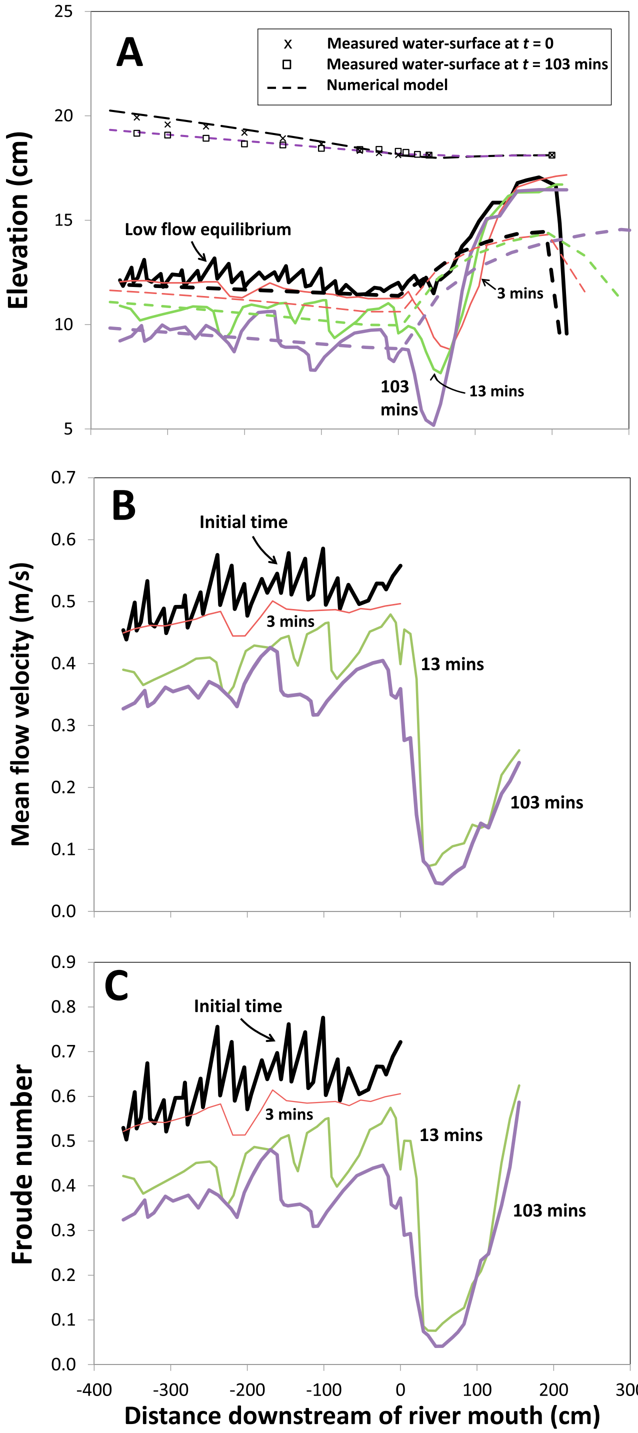

Figure 8. Experimental results from Experiment 4 (high-flow transient; solid lines) starting from low-flow equilibrium conditions (black lines) for (a) bed and water surface elevations, (b) mean flow velocity, and (c) Froude number. Dashed lines are from the numerical model. Flow is from left to right. The vertical axis is referenced to the flume bottom.

flume. For example, numerical modeling indicates that we would expect no change in bed topography within our flume (-4.5 m $< x < 0$) for the first 13.5 h of runtime of Experiment 3 because the downstream migrating depositional wedge would be upstream of the length of our flume and bed shear stresses within -4.5 m $< x < 0$ would be below the threshold of motion (Figure 4a). This is better illustrated in Figure 6 which shows that the expected sediment flux at $x = -4.5$ m (i.e., the upstream extent of our flume experiments and location of the sediment feeder) changes as a function of time, despite that the sediment supply at the upstream end of the numerical model domain is constant and set to the sediment transport capacity (i.e., equation (6)). To simulate the full backwater zone, we used the numerical model output in Figure 6 to prescribe the time evolution of sediment supply at the upstream end of our flume. The model output was discretized into two feed rates for Experiment 3 (with the first feed rate set to zero) and four feed rates for Experiment 4 (Figure 6).

Results show that it took the low-flow case about 21.5 h to fill in the scoured bed topography left behind from the previous high-flow case (Figure 7a). The adjustment of the bed occurred through a downstream migrating wedge of sediment, which matches well with the expectation from the numerical simulations (Figure 7a). No bed adjustment occurred in the experiment for the first 13.5 h of the experiment as sediment feed was zero (Figure 6a) and bed shear stresses were below the threshold of motion everywhere. The prograding wedge of sediment reached the river mouth at about 17.5 h, and it took another 4 hours for the flow to fill in the offshore scour hole generated by the previous high-flow event. The mean flow velocity in the river channel section ($x < 0$) showed strong spatial deceleration with velocities about ~ 0.24 m/s upstream of the propagating sediment wedge, and ~ 0.12 m/s downstream of the wedge as a result of the two-fold decrease in-channel depth from channel-bed aggradation. Like the equilibrium Experiment 1, spreading of the offshore plume resulted in spatial deceleration of flow along

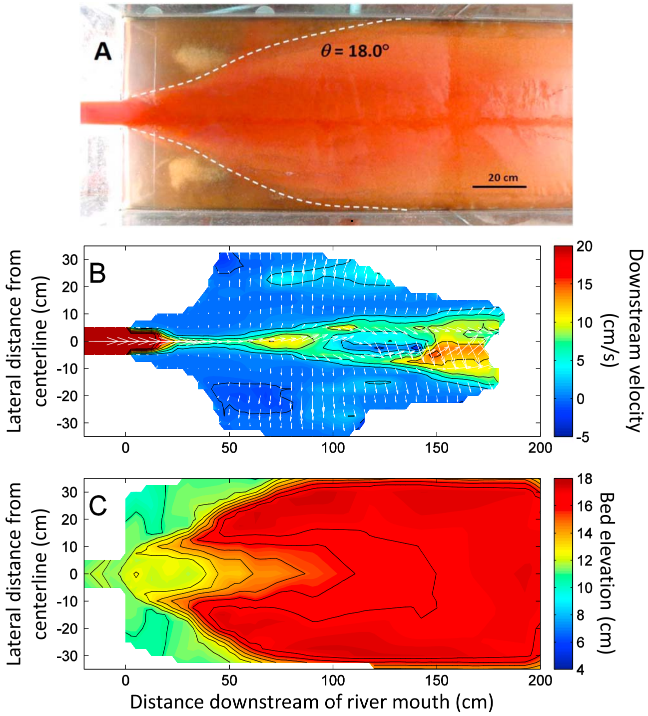

Figure 9. Plan view of results from the end of Experiment 1 (low-flow equilibrium) at $t = 10.5$ h, showing (a) an image of the spreading plume with red dye, (b) surface flow velocity where colors denote the magnitude of the downstream component of velocity and the white arrows show the full velocity field, and (c) bed elevation. The water surface in the basin was at 18.3 cm elevation. Only the lowermost part of the river section and the basin are shown (-20 cm $< x <$ 200 cm).

the plume centerline (Figure 7b); however, offshore deposition did not occur until ~ 20 h of runtime as sediment before then was sequestered upstream. The measured Froude numbers were subcritical during transient adjustment (Figure 7c).

For Experiment 4, the final bed topography from Experiment 3 was used as the initial condition, and the water and sediment supply conditions were set to the high-flow case (Table 1). Transient adjustment of the bed was rapid with a 3 cm deep scour hole developing just offshore of the river mouth within 3 min (Figure 8a). After 13 min of runtime, the upstream migrating erosional wave reached the upstream end of the flume, and by 103 min the bed topography approached that observed in the equilibrium case. The adjustment of the bed topography was accompanied by an adjustment of the water surface from a steeper profile (indicative of drawdown; e.g., Figure 4d) during the beginning of the run ($S = 0.0044$), to a lower sloping water surface profile ($S = 0.0028$) toward the end of the run that approached the equilibrium value of 0.0015. Erosion of the bed was driven by spatial acceleration of flow from 0.45 m/s at $x = -3.6$ m to 0.56 m/s at the river mouth ($x = 0$) at $t = 3$ min (Figure 8b). As the riverbed approached its equilibrium configuration, the water velocity was nearly spatially uniform, except in the offshore region where plume spreading resulted in spatial deceleration of flow along the plume centerline for $0 < x < 60$ cm, and spatial acceleration farther downstream (Figure 8b). The Froude number was the greatest during the early stages of transient adjustment of the bed due to the inherited elevated bed topography at the river mouth but was still subcritical at all times ($Fr < 0.75$) (Figure 8c). Note that the scoured channel observed just offshore of the river mouth in Experiment 2 also occurred in this experiment and enlarged in time reaching a total length of ~ 0.8 m and a depth of ~ 4 cm at the end of the experiment (Figure 8a).

5.3. Morphodynamics in the Offshore Basin

Morphodynamics offshore of the river mouth were governed by the spreading plume, bed erosion and deposition, and the interaction between the two. For example, Figure 9 shows the river plume, flow velocity, and bed topography at the end of Experiment 1. The spreading angle of the plume (~18°, Figure 9a) is larger than expected from classic turbulent jet theory [e.g., *Rajaratnam*, 1976] (i.e., 5.7° for width-averaged velocity profile), presumably due to the fan-shaped deposit (Figure 9c) that forced lateral spreading of the plume (Figure 9b). The jets were also unstable in that meandering and large-scale coherent flow structures developed along the plume boundaries [e.g., *Jirka*, 2001; *Landel et al.*, 2012]. The jet-stability parameter for our high- and low-flow cases was 0.0096 and 0.013, respectively, and plots correctly in the unstable (meandering) regime of *Canestrelli et al.* [2014]. Jet meandering, when it occurs, is thought to dominate mixing [*Rowland et al.*, 2009; *Landel et al.*, 2012] and govern subaqueous levee deposition along the jet margins [*Rowland et al.*, 2010; *Mariotti et al.*, 2013]. There were upstream-oriented velocities in all the experiments to the sides of the plume (e.g., Figure 9b) as expected from entrainment of ambient water into the plume. The strength of this return flow was likely influenced by the walls in our flume, but the return-flow velocities were typically small compared to those along the plume centerline suggesting that wall effects were minor.

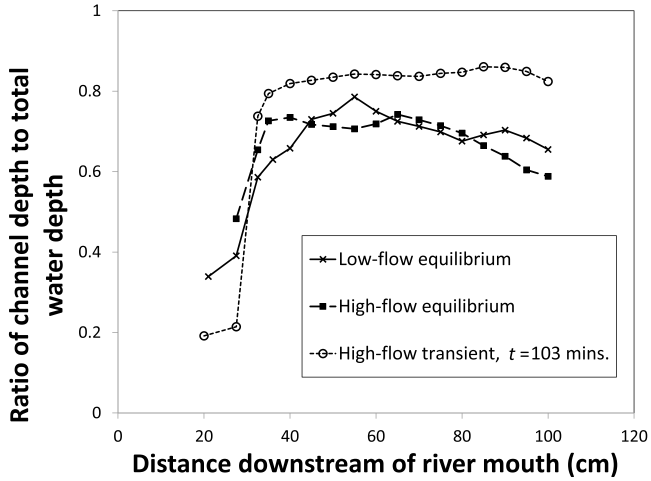

Figure 10. Plot of the ratio of channel depth (difference between levee top and thalweg elevation) to total water depth (difference between the water surface and the thalweg depth) along the plume centerline in the offshore basin for Experiments 1, 2, and 4. The values from Experiment 3 are omitted here since they are similar to Experiment 2.

The offshore deposit showed the characteristic shape of bed elevation increasing downstream from the river mouth (Figure 9c). Deposition rates were the largest along the margins of the plume resulting in the formation of levees that grew to within 1 cm of the water surface in places (e.g., $x = 90$ cm in Figure 9c) and nearly completely confined the flow within a channel. At the distal end of the basin ($x > 150$ cm), deposition resulted in very shallow flow depths (<1 cm) (Figure 9c). Levee deposition was absent near the river mouth ($0 < x < 15$ cm), and channelization ceased due to infilling at the distal end of the flume (Figure 9c). Except for a small region near the river mouth, the plume was approximately 70% confined over its water depth by the leveed topography (Figure 10).

For the high-flow equilibrium run (Experiment 2) after $t = 7.25$ h, plume spreading was 10.2° (Figure 11a), smaller than that observed in Experiment 1. The enhanced confinement of the plume relative to Experiment 1 is likely a result of scour into the bed resulting in a well-defined submarine channel from 5 cm $< x <$ 85 cm (Figure 11c). The plume had high-flow velocities along the centerline, with spreading and return flow beyond the margins of the channel (Figure 11b). The self-formed channel had greater relief in Experiment 2 as compared to Experiment 1, but the relative confinement over the total water depth was similar between the two cases (Figure 10).

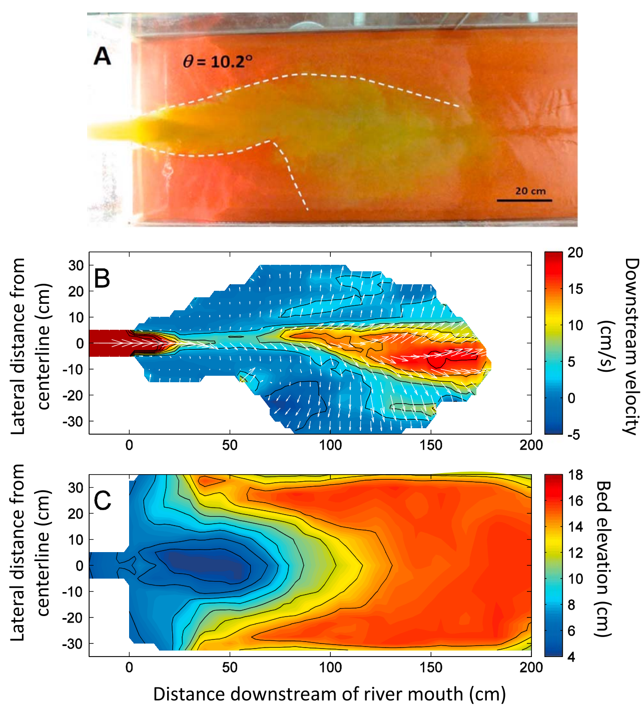

Figure 11. Plan view of results from the end of Experiment 2 (high-flow equilibrium) at $t = 7.25$ h, showing (a) an image of the spreading plume with red dye, (b) surface flow velocity where colors denote the magnitude of the downstream component of velocity and the white arrows show the full velocity field, and (c) bed elevation where the water surface in the basin was at 18.3 cm. Only the lowermost part of the river section and the basin are shown (−20 cm $< x <$ 200 cm).

Figure 12 shows the results from Experiment 3 where the low-flow case filled the inherited topography from the high-flow case of Experiment 2. After $t = 15.0$ h in Experiment 3 (which corresponds to 1.5 h since the onset of sediment feed and topographic change; Figure 6a), plume spreading was reduced to 13.2° as compared to 18° from Experiment 1, presumably due to corralling of the flow from the inherited scoured channel from Experiment 2. Transient filling of the inherited channel occurred by deposition along the channel thalweg and levee growth (e.g., shown at two cross sections $x = 36$ cm and $x = 94$ cm in Figure 13). At $x = 36$ cm, levee deposition outpaced thalweg deposition resulting in temporal increase in the degree of channelization

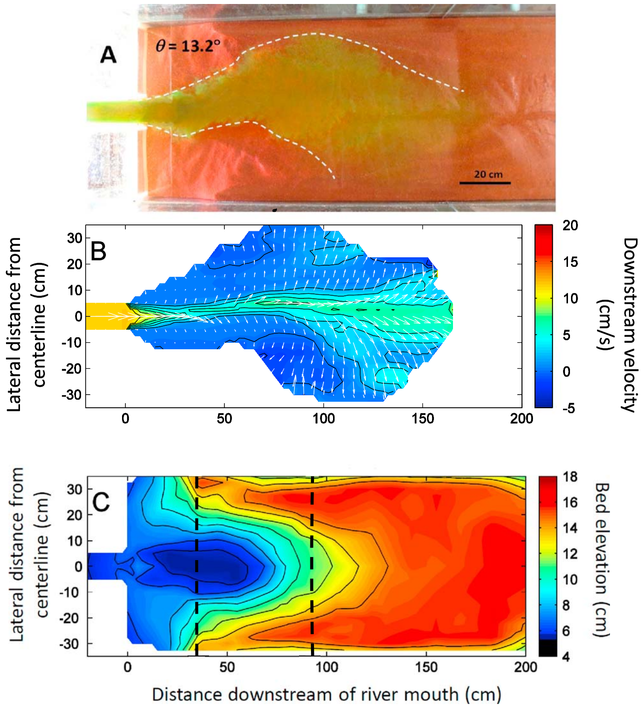

Figure 12. Plan view of results from the Experiment 3 (low-flow transient) at $t = 15.0$ h showing (a) an image of the spreading plume with red dye, (b) surface flow velocity where colors denote the magnitude of the downstream component of velocity and the white arrows show the full velocity field, and (c) bed elevation where the water surface in the basin was at 18.3 cm. Only the lowermost part of the river section and the basin are shown (-20 cm $< x <$ 200 cm). The scour hole is from the previous run (Figure 11c). The dashed lines are locations of cross sections in Figure 13.

(Figures 12 and 13a), whereas at $x = 94$ cm channelization diminished in time owing to thalweg deposition that outpaced levee deposition (Figures 12 and 13b). The resulting channel for the low-flow case was narrower than the inherited channel from the high-flow case (Figure 13a).

Figure 14 shows results from the beginning of Experiment 4 where the high-flow event scoured into the inherited topography produced by the low-flow event of Experiment 3. Unlike Experiment 3, here channelization was driven mostly by scour into the underlying deposit along the plume centerline rather than by levee deposition (Figure 14c). Channelization led to heightened velocities along the plume centerline (Figure 14b) and the greatest degree of plume confinement (spreading angle of 7.7°) observed in any of the experiments. In this experiment the relief of the scoured channel was greater than that in Experiment 2 (i.e., equilibrium high-discharge case that started with a flat bed) due to the high elevation of the initial bed inherited from the previous, low-flow experiment. Thus, in these experiments, a cycle of high- and low-flow events led to enhanced channelization as compared to one flow event alone, with the channelized depth exceeding 80% of the total water depth over most of the delta (Figure 10). Cross sections through the evolving bed topography at both $x = 36$ cm and $x = 94$ cm show scouring along the channel centerline, widening of the channel, and little levee deposition (Figures 13c and 13d).

6. Discussion

6.1. The Persistence of Backwater Zones

Upstream of the backwater zone, alluvial rivers typically respond to a river flood by increasing water depth (accommodated by an increase in water surface elevation) and increasing sediment transport capacity. If sediment supply changes commensurate to the transport capacity (as designed in our flume experiments), and in the absence of subsidence and sea level rise, then no riverbed erosion or deposition should occur [e.g., *Lane*, 1955]. Our experiments show that this logic does not hold near the river mouth because spreading of the offshore plume renders the water surface elevation there nearly fixed at sea level (e.g., Figure 8a). Any substantial increase in water depth at the river mouth must be accommodated by lowering the bed rather than raising the water surface. Thus, the shared river mouth boundary condition between river and river plume makes erosion and deposition patterns in coastal rivers particularly sensitive to floods of different discharge and may lead to a persistent backwater zone.

Lane [1957] observed that many rivers including the Mississippi River and those that enter the Great Lakes of North America are much deeper near their mouths than farther upstream resulting in natural fluvial harbors. He claimed that this must be the result of infrequent large flow events that focus scour near river mouths, and that the natural harbors remain deep for a long period of time. In our study, both numerical model results (Figure 4) and flume experimental results (Figures 7a and 8a) demonstrate a persistent backwater zone due to the alternation of low-flow and high-flow events. The high flows scour the bed upstream of the river mouth

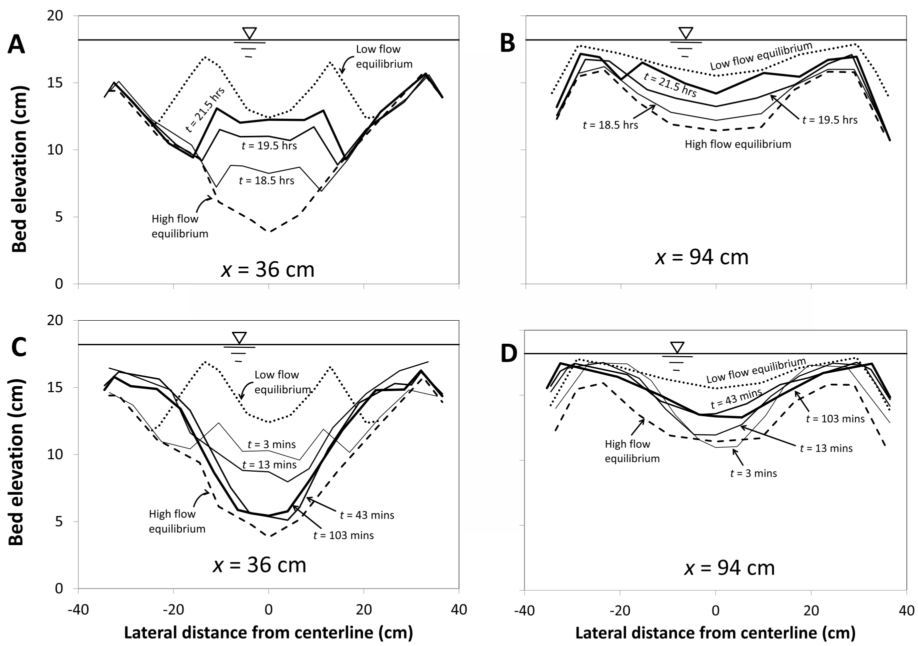

Figure 13. Cross-sectional profiles illustrating the bed evolution during (a, b) Experiment 3 and (c, d) Experiment 4 at two different cross-section locations (x = 36 cm and 94 cm; see Figures 12c and 14c for locations). Experiment 3, as shown in Figures 13a and 13b, shows the bed transitioning from high-flow equilibrium (dashed lines) to low-flow equilibrium (dotted lines) and at time steps t = 18.5, 19.5, and 21.5 h. For experiment 4, as shown in Figures 13c and 13d, the bed transitioned from the low-flow equilibrium case (dotted lines) to the high-flow equilibrium (dashed lines) and profiles are shown at time steps t = 3, 13, 43, and 103 min.

which creates nonuniform flow at low discharges, and the low-discharge events deposit sediment in the backwater zone which creates nonuniform flow at high discharges. In the absence of flow-discharge alternations, our experiments show that the bed evolves to a state of normal flow and sediment bypass, where deviations from this state are due only to propagation of the delta front.

The characteristic timescale for the bed to evolve to reach near normal-flow, sediment-bypass conditions can be long for natural rivers. For example, *Chatanantavet et al.* [2012] used a quasi-2-D river plume morphodynamic model and found that the backwater zone in the Mississippi River (~450 km upstream from the river mouth) persists over thousands of years because the timescale of discharge variation (e.g., floods of morphodynamic significance for both bed erosion and deposition occur at near annual timescales) is small compared to the characteristic timescale for the bed to adjust to a given flow event (~10^2 years).

To derive a rough scale for the time (t_{adj}) for a lowland riverbed to come into equilibrium with imposed discharge and sediment flux conditions over the backwater zone (e.g., Figure 4), we consider mass balance

$$t_{\mathrm{adj}} \propto \frac{(1-\lambda_p)L\Delta z}{q_{s,n}} \tag{6}$$

in which the bed adjustment time is proportional to the volume of sediment-bed change per unit width (i.e., $(1-\lambda_p)L\Delta z$, where L is the length of the backwater zone (Figure 1) and Δz is the amount of vertical channel-bed change) normalized by the input sediment flux per unit width for normal-flow conditions (i.e., upstream of the backwater zone), $q_{s,n}$. Without information on the exact discharge and sediment flux of a particular event, we propose that the amount of vertical channel-bed change for a given river scales approximately with the characteristic flow depth for that river, or in other words $\Delta z \propto h_n$, where h_n is the normal-flow depth. Also, noting that the backwater length scales to first order like $L \propto h_n/S$ [e.g., *Parker*, 2004; *Lamb et al.*, 2012], where S is the bed slope, equation (6) can be rewritten as

$$t_{\mathrm{adj}} \propto \frac{(1-\lambda_p)h_n^2}{S\, q_{s,n}}. \tag{7}$$

The variables in equation (7) can be found for a number of rivers assuming that normal-flow conditions are reflected by bankfull or 2 year recurrence floods [e.g., *Parker*, 2004].

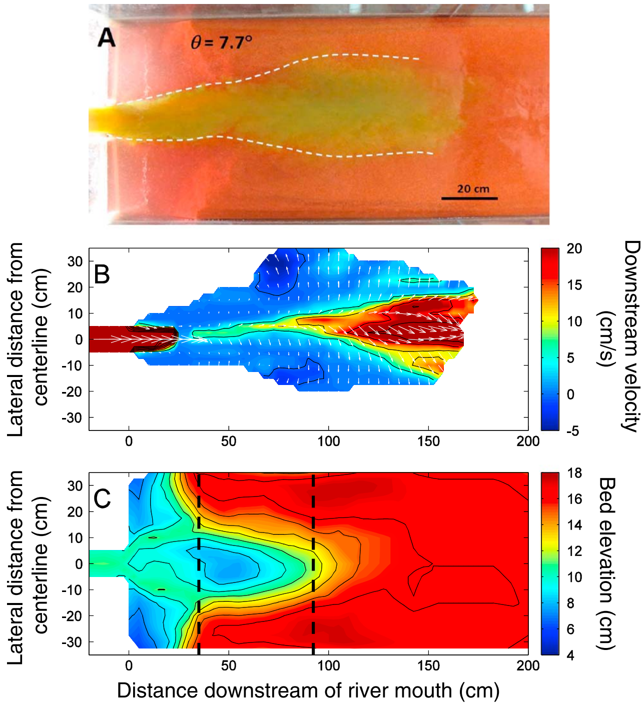

Figure 14. Plan view of results from the beginning of Experiment 4 (high-flow transient) at $t = 13$ min, showing (a) an image of the spreading plume with red dye, (b) surface flow velocity where colors denote the magnitude of the downstream component of velocity and the white arrows show the full velocity field, and (c) bed elevation where the water surface in the basin was at 18.3 cm. Only the lowermost part of the river section and the basin are shown (-20 cm $< x <$ 200 cm). The dashed lines are locations of cross sections in Figure 13.

Using equation (7), the characteristic timescale of adjustment for our low-flow and high-flow cases is estimated at 45 and 95 h, respectively, which roughly matches the calculated time for complete bed adjustment of 20 and 79 h based on the full numerical model (Figure 15). We estimated the adjustment timescale for four natural rivers in which bed material transport rates for the bankfull (normal) flows were estimated using *Engelund and Hansen* [1967] and grain sizes for these rivers were obtained from *Syvitski* [2005], as well as water discharge from Oak Ridge National Laboratory Distributed Active Archive Center (Figure 15). Like the Mississippi River, most of these rivers yield characteristic bed adjustment timescales on the order of multiple years to multiple decades. This suggests that nonuniform flow, transient bed adjustment, and persistent backwater zones, rather than normal-flow conditions, are likely to prevail in the lowermost portions of rivers.

6.2. Levees, Scour, and Self-Channelization

For subaqueous levee formation, *Wright* [1977] suggested that flows in contact with the bed would be friction dominated and spread rapidly; hence, they should have rapidly diverging levees and mouth bars. In contrast, *Rowland et al.* [2010] conducted physical experiments on subaqueous levee development from a sediment-laden homopycnal jet entering a basin of still water on a fixed, nonerodible bed. They found that levees were nearly parallel in cases, and they emphasized the role of lateral transport of suspended sediment—from the plume centerline to its margins-driven by turbulence and meandering associated with jet instability. Similar results have been produced in more recent 2-D numerical models suggesting that levee deposition is tied to jet instability [*Canestrelli et al.*, 2014], which is related mathematically to jet potential vorticity [*Falcini et al.*, 2014], and sediment near the threshold of suspension [*Mariotti et al.*, 2013]. Our results for low-flow conditions (e.g., Figure 9c) are consistent with these recent experimental and numerical findings for the formation of subaqueous levees.

However, our results for high-flow cases differ significantly from previous work that we observed scour along the centerline of the jet into the underlying alluvial bed. In the experiments of *Rowland et al.* [2010], their nonerodible bed was often devoid of sediment along the jet centerline suggesting that scour might have occurred in their experiments as well if the bed had been alluvial. Scour from planar jets has been observed before in experiments designed for various engineering applications [e.g., *Rajaratnam and Berry*, 1977; *Rajaratnam*, 1981; *Rajaratnam and Macdougall*, 1983; *Mason and Arumugam*, 1985; *Hogg et al.*, 1997; *Dey and Sarkar*, 2006; *Faruque et al.*, 2006; *Sui et al.*, 2008]. However, these previous experiments on jet scour used clear-water inputs with no sediment feed; thus, the flows were under capacity with respect to sediment transport and were therefore expected to entrain sediment, despite spatial deceleration, as long as the threshold for entrainment was surpassed. *Hogg et al.* [1997], for example, reported that grains are eroded if the shear stress exerted on the surface of the bed exceeds the critical stress for motion.

The observation of offshore ($0 < x < 85$ cm) bed scour during high flows in our experiments is surprising, however, because our river plumes were fed by an extensive feeder river with an alluvial bed and were thus

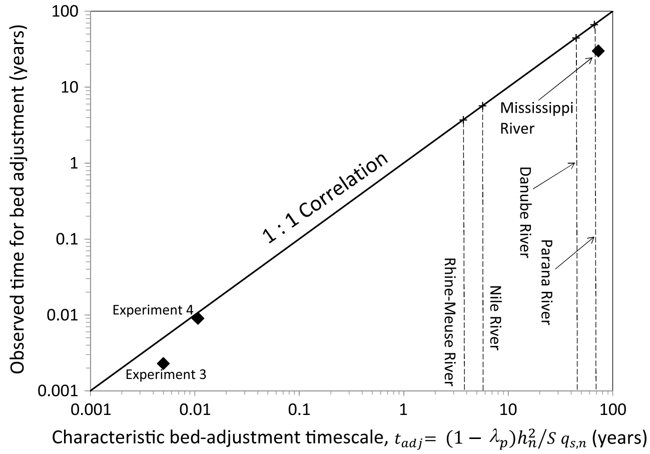

Figure 15. Observed bed adjustment time versus the characteristic bed adjustment time (t_{adj}) inferred from a scaling analysis (section 6.1). Symbols show the observed adjustment times for the transient experiments presented herein (Experiments 3 and 4) and an inferred/calculated adjustment time for the lower Mississippi River based on the numerical morphodynamic modeling of *Chatanantavet et al.* [2012]. Calculated timescales for other rivers are given for comparison. The characteristic bed adjustment timescales (t_{adj}) were calculated for the Rhine-Meuse River using $h_n = 5.0$ m, $q_{s,n} = 6.5 \times 10^4$ t/yr/m, $S = 1.1 \times 10^{-4}$, $Q_w = 5750$ m^3/s [*Jerolmack and Mohrig*, 2007]; for the Nile River using $h_n = 16.2$ m, $q_{s,n} = 7.7 \times 10^5$ t/yr/m, $S = 6.4 \times 10^{-5}$, $Q_w = 8800$ m^3/s [*Saad*, 2002]; for the Danube River using $h_n = 6.3$ m, $q_{s,n} = 1.9 \times 10^4$ t/yr/m, $S = 5.0 \times 10^{-5}$, $Q_w = 9700$ m^3/s [*Giosan et al.*, 2005; *Opreanu*, 2010]; and for the Parana River using $h_n = 11.8$ m, $q_{s,n} = 5.5 \times 10^4$ t/yr/m, $S = 4.0 \times 10^{-5}$, $Q_w = 22{,}800$ m^3/s [*Depetris and Gaiero*, 1998].

likely transporting sediment at their capacity. In addition, we observed marked spatial deceleration in the river plume along the centerline, and therefore would have expected rapid deposition of sediment in the same region due to loss of transport capacity (despite that shear stresses exceeded the threshold for sediment motion). The scour cannot be reproduced by our quasi-2-D, depth-averaged numerical model, and it has yet to be produced in more sophisticated 2-D numerical models and emerging theories [e.g., *Edmonds and Slingerland*, 2007; *Mariotti et al.*, 2013; *Canestrelli et al.*, 2014; *Falcini et al.*, 2014], and so this suggests that 3-D morphodynamics led to the scoured bed. Field observations also indicate that regions of strong flow divergence, like bifurcations on deltas and within subaqueous channels, can show bed scour [e.g., *Shaw et al.*, 2013; *Shaw and Mohrig*, 2013].

It is possible that the observed bed erosion in our experiments occurred due to lateral sediment transfer as a result of turbulent mixing, similar to the mechanism proposed by *Rowland et al.* [2010]. Another possibility is that strong secondary currents formed under the lateral spreading mound of water, perhaps creating a pair of helical vortices sweeping sediment along the bed from the center of the plume to the levees, as has been shown for river confluences [e.g., *Ashmore and Parker*, 1983; *Best and Ashworth*, 1997]. Limited 3-D velocity data in wall-bounded jets indicate the tendency for flow to sweep outward along the bed from the jet centerline to the jet margins [*Foss and Jones*, 1968; *Holdeman and Foss*, 1975; *Shinneeb et al.*, 2010], although data from *Rowland et al.* [2009, their Figure 9] suggest an opposite sense of secondary circulation. The region of observed offshore scour in our experiments also correlates with the zone of flow establishment (ZOFE) for jets, typically reported to be around five to nine channel widths [e.g., *Bates*, 1953; *Rowland et al.*, 2009]. Within the ZOFE enhanced shear may result in enhanced transport near the bed. Finally, the M2-drawdown dynamics observed in the river section during high flows may have translated downstream of the imposed river mouth, or through erosion at the river mouth, directed the jet obliquely into the offshore bed resulting in enhanced sediment transport capacity. This last mechanism suggests a strong coupling between fluvial backwater dynamics and offshore depositional patterns, a potential coupling that has not been addressed in previous modeling and experimental work on river mouth deposits [e.g., *Edmonds and Slingerland*, 2007; *Rowland et al.*, 2010; *Falcini and Jerolmack*, 2010; *Mariotti et al.*, 2013; *Canestrelli et al.*, 2014; *Falcini et al.*, 2014].

Whatever the cause of offshore erosion by the river plume in our experiments, it is clear that the alternations of transient fill and levee deposition during low flow and thalweg scour during high flow led to a greater degree of self-channelization (up to 85%; Figures 10 and 13). In contrast, our results from the equilibrium runs (single flow events) are similar to that of *Rowland et al.* [2009] in that levees ceased to grow after they confined ~75% of the flow. The importance of variable flow conditions and erosion in self-channelization is supported by recent observations of Wax Lake Delta, USA, where channelization is partly attributed to channel-bed erosion offshore of the river mouth induced by variable flood and tidal conditions [*Shaw et al.*, 2013; *Shaw and Mohrig*, 2013]. Thus, multiple flood events and the potential for erosion may need to be assessed in emerging theories for self-channelization of planar jets [e.g., *Falcini et al.*, 2014; *Canestrelli et al.*, 2014] and the formation of elongate deltas [e.g., *Kim et al.*, 2009b].

7. Conclusion

Our numerical model and flume results demonstrate that during low flows backwater hydrodynamics cause spatial-flow deceleration and a downstream-propagating wave of bed deposition, and during high flows the backwater zone becomes a region of water surface drawdown, spatial-flow acceleration and bed scour. Thus, bed aggradation and degradation within coastal rivers can occur due to nonuniform flow dynamics imposed by boundary conditions set by the coupled offshore plume, even in the absence of subsidence, sea level rise, or changes in the ratio of sediment supply to transport capacity of the upstream feeder river. We derived a characteristic timescale for riverbed adjustment within the backwater zone and found, when upscaled to natural systems, that most coastal rivers should be in a state of transient bed adjustment, where floods of geomorphic significance occur too frequently to reach quasi-normal-flow and sediment-bypass conditions, and the net result is a persistent hydrodynamic backwater zone. Our experiments also show that variable flood discharges can lead to enhanced channelization of the offshore plume through both levee deposition and channel-bed erosion. Although deltas are net-depositional landforms, our results suggest that transient erosion during floods may play an important role in forming distributary networks and therefore delta morphology and stratigraphy.

Acknowledgments
We thank Brian Fuller and Aaron Tran for assisting with parts of the flume experiments. Our analysis benefited from informal discussions with Joel Rowland. This work was funded by the U.S. National Science Foundation grant OCE-1233685 and the American Chemical Society Petroleum Research Fund to MPL. We thank Editor A. Densmore, Associate Editor W. Kim, J. Nittrouer, F. Falcini, and J. Martin for constructive comments on a previous draft. Data sets used to produce the results of this paper have been curated, and readers are encouraged to contact the first author (P.C.) if interested in the data, or visit https://sites.google.com/site/sedimentexperimentalists/home (then click "Materials" and "Interactive data folder"), with no restrictions on access.

References

Allison, M. A., T. M. Dellapenna, E. S. Gordon, S. Mitra, and S. T. Petsch (2010), Impact of Hurricane Katrina (2005) on shelf organic carbon burial and deltaic evolution, *Geophys. Res. Lett.*, *37*, L21605, doi:10.1029/2010GL044547.

Ashmore, P., and G. Parker (1983), Confluence scour in coarse braided streams, *Water Resour. Res.*, *19*(2), 392–402, doi:10.1029/WR019i002p00392.

Bagnold, R. A. (1956), The flow of cohesionless grains in fluids, *Philos. Trans. R. Soc. London, Ser. A*, *249*(964), 235–297.

Bates, C. C. (1953), Rational theory of delta formation, *Am. Assoc. Pet. Geol. Bull.*, *37*, 2119–2162.

Best, J. L., and P. J. Ashworth (1997), Scour in large braided rivers and the recognition of sequence stratigraphic boundaries, *Nature*, *387*, 275–277, doi:10.1038/387275a0.

Blum, M. D., and H. H. Roberts (2009), Drowning of the Mississippi Delta due to insufficient sediment supply and global sea-level rise, *Nat. Geosci.*, *2*, 488–491, doi:10.1038/ngeo553.

Blum, M. D., and T. E. Tornqvist (2000), Fluvial responses to climate and sea-level change: A review and look forward, *Sedimentology*, *47*, 2–48.

Blum, M. D., J. Martin, K. Milliken, and M. Garvin (2013), Paleovalley systems: Insights from Quaternary analogs and experiments, *Earth Sci. Rev.*, *116*, 128–169, doi:10.1016/j.earscirev.2012.09.003.

Bresse, J. A. C. (1860), *Cours de Mecanique Appliquee, Hydraulique*, 2nd ed., Mallet-Bachelier, Paris, France.

Canestrelli, A., W. Nardin, D. Edmonds, S. Fagherazzi, and R. Slingerland (2014), Importance of frictional effects and jet instability on the morphodynamics of river mouth bars and levees, *J. Geophys. Res. Oceans*, *119*, 509–522, doi:10.1002/2013JC009312.

Chatanantavet, P., M. P. Lamb, and J. A. Nittrouer (2012), Backwater controls of avulsion location on deltas, *Geophys. Res. Lett.*, *39*, L01402, doi:10.1029/2011GL050197.

Chow, V. T. (1959), *Open Channel Hydraulics*, 680 pp., McGraw Hill, U.S.A.

Depetris, P. J., and D. M. Gaiero (1998), Water-surface slope, total suspended sediment and particulate organic carbon variability in the Parana River during extreme flooding, *Naturwissenschaften*, *85*, 26–28.

Dey, S., and A. Sarkar (2006), Scour downstream of an apron due to submerged horizontal jets, *J. Hydraul. Eng.*, *132*(3), 246–257.

Edmonds, D. A., and R. L. Slingerland (2007), Mechanics of river mouth bar formation: Implications for the morphodynamics of delta distributary networks, *J. Geophys. Res.*, *112*, F02034, doi:10.1029/2006JF000574.

Edmonds, D. A., and R. L. Slingerland (2008), Stability of delta distributary networks and their bifurcations, *Water Resour. Res.*, *44*, W09426, doi:10.1029/2008WR006992.

Edmonds, D. A., and R. L. Slingerland (2010), Significant effect of sediment cohesion on delta morphology, *Nat. Geosci.*, *3*, 105–109, doi:10.1038/ngeo730.

Edmonds, D., R. Slingerland, J. Best, D. Parsons, and N. Smith (2010), Response of river-dominated delta channel networks to permanent changes in river discharge, *Geophys. Res. Lett.*, *37*, L12404, doi:10.1029/2010GL043269.

Engelund, F., and E. Hansen (1967), *A Monograph on Sediment Transport in Alluvial Streams*, Teknisk Forlag, Copenhagen, Denmark.

Falcini, F., and D. J. Jerolmack (2010), A potential vorticity theory for the formation of elongate channels in river deltas and lakes, *J. Geophys. Res.*, *115*, F04038, doi:10.1029/2010JF001802.

Falcini, F., A. Piliouras, R. Garra, A. Guerin, D. J. Jerolmack, J. Rowland, and C. Paola (2014), Hydrodynamic and suspended sediment transport controls on river mouth morphology, *J. Geophys. Res. Earth Surf.*, *119*, 1–11, doi:10.1002/2013JF002831.

Faruque, M. A. A., P. Sarathi, and R. Balachandar (2006), Clear water local scour by submerged three-dimensional wall jets: Effect of tailwater depth, *J. Hydraul. Eng.*, *132*(6), 575–580.

Flemings, P. B., and T. E. Jordan (1989), A synthetic stratigraphic model of foreland basin development, *J. Geophys. Res.*, *94*(B4), 3851–3866, doi:10.1029/JB094iB04p03851.

Foss, J. F., and J. B. Jones (1968), Secondary flow effects in a bounded rectangular jet, *J. Basic Eng.*, *90*(2), 241–248.

Galler, J. J., T. S. Bianchi, M. A. Allison, L. A. Wysocki, and R. Campanella (2003), Biogeochemical implications of levee confinement in the lowermost Mississippi River, *Eos Trans. AGU*, *84*(44), 469–476, doi:10.1029/2003EO440001.

Geyer, W. R., P. S. Hill, and G. C. Kineke (2004), The transport, transformation and dispersal of sediment by buoyant coastal flows, *Cont. Shelf Res.*, *24*, 927–949.

Giosan, L., J. P. Donnelly, E. Vespremeanu, J. P. Bhattacharya, C. Olariu, and F. S. Buonaiuto (2005), River delta morphodynamics: Examples from the Danube Delta, in *River Deltas—Concepts, Models, and Examples*, *SEPM Spec. Publ.*, vol. 83, pp. 393–411, Society for Sedimentary Geology.

Hetland, R. D. (2010), The effects of mixing and spreading on density in near-field river plumes, *Dyn. Atmos. Oceans*, *49*(1), 37–53.

Hetland, R. D., and D. G. MacDonald (2008), Spreading in the near-field Merrimack River plume, *Ocean Modell.*, *21*(1), 12–21.

Hogg, A. J., H. E. Huppert, and W. B. Dade (1997), Erosion by planar turbulent wall jets, *J. Fluid Mech.*, *338*, 317–340.
Holdeman, J. D., and J. F. Foss (1975), The initiation, development, and decay of the secondary flow in a bounded jet, *J. Fluids Eng.*, *97*(3), 342–352.
Hotchkiss, R. H., and G. Parker (1991), Shock fitting of aggradational profiles due to backwater, *J. Hydraul. Eng.*, *117*, 1129–1144.
Hoyal, D., and B. A. Sheets (2009), Morphodynamic evolution of experimental cohesive deltas, *J. Geophys. Res.*, *114*, F02009, doi:10.1029/2007JF000882.
Jerolmack, D. J. (2009), Conceptual framework for assessing the response of delta channel networks to Holocene sea level rise, *Quat. Sci. Rev.*, *28*(17–18), 1786–1800, doi:10.1016/j.quascirev.2009.02.015.
Jerolmack, D. J., and D. Mohrig (2007), Conditions for branching in depositional rivers, *Geology*, *35*(5), 463–466, doi:10.1130/G23308A.1.
Jerolmack, D. J., and J. B. Swenson (2007), Scaling relationships and evolution of distributary networks on wave-influenced deltas, *Geophys. Res. Lett.*, *34*, L23402, doi:10.1029/2007GL031823.
Jirka, G. H. (2001), Large scale flow structures and mixing processes in shallow flows, *J. Hydraul. Res.*, *39*(6), 567–573, doi:10.1080/00221686.2001.9628285.
Karadogan, E., C. S. Willson, and C. R. Berger (2009), Numerical modeling of the Lower Mississippi River—Influence of forcings on flow distribution and impact of sea level rise on the system, in *OCEANS 2009, MTS/IEEE Biloxi - Marine Technology for Our Future: Global and Local Challenges*, pp. 1–7, The Institute of Electrical and Electronics Engineers, Biloxi, MS.
Kim, W., D. Mohrig, R. Twilley, C. Paola, and G. Parker (2009a), Is it feasible to build new land in the Mississippi River Delta?, *Eos Trans. AGU*, *90*(42), 373–374, doi:10.1029/2009EO420001.
Kim, W., A. Dai, T. Muto, and G. Parker (2009b), Delta progradation driven by an advancing sediment source: Coupled theory and experiment describing the evolution of elongated deltas, *Water Resour. Res.*, *45*, W06428, doi:10.1029/2008WR007382.
Kim, W., B. A. Sheets, and C. Paola (2010), Steering of experimental channels by lateral basin tilting, *Basin Res.*, *22*, 286–301, doi:10.1111/j.1365-2117.2009.000419.x.
Lamb, M. P., and D. Mohrig (2009), Do hyperpycnal-plume deposits record river-flood dynamics?, *Geology*, *7*(12), 1067–1070, doi:10.1130/G30286A.
Lamb, M. P., B. McElroy, B. Kopriva, J. Shaw, and D. Mohrig (2010), Linking river-flood dynamics to hyperpycnal-plume deposits: Experiments, theory, and geological implications, *Geol. Soc. Am. Bull.*, *122*(9/10), 1389–1400, doi:10.1130/B30125.1.
Lamb, M. P., J. A. Nittrouer, D. Mohrig, and J. Shaw (2012), Backwater and river plume controls on scour upstream of river mouths: Implications for fluvio-deltaic morphodynamics, *J. Geophys. Res.*, *117*, F01002, doi:10.1029/2011JF002079.
Landel, J. R., C. P. Caulfield, and A. W. Woods (2012), Meandering due to large eddies and the statistically self-similar dynamics of quasi-two-dimensional jets, *J. Fluid Mech.*, *692*, 347–368, doi:10.1017/jfm.2011.518.
Lane, E. W. (1955), The importance of fluvial morphology in hydraulic engineering, *Proc. Am. Soc. Civil Eng.*, *81*(745), 1–17.
Lane, E. W. (1957), *A Study of the Shape of Channels Formed by Natural Streams Flowing in Erodible Material*, M.R.D. Sediment Ser., vol. 9, 170 pp., U.S. Army Engineer Division, Missouri River, Corps of Engineers, Omaha, Nebr.
MacDonald, D. G., and W. R. Geyer (2004), Turbulent energy production and entrainment at a highly stratified estuarine front, *J. Geophys. Res.*, *109*, C05004, doi:10.1029/2003JC002094.
Mariotti, G., F. Falcini, N. Geleynse, M. Guala, T. Sun, and S. Fagherazzi (2013), Sediment eddy diffusivity in meandering turbulent jets: Implications for levee formation at river mouths, *J. Geophys. Res. Earth Surf.*, *118*, 1908–1920, doi:10.1002/jgrf.20134.
Mason, P. J., and K. Arumugam (1985), Free jet scour below dams and flip buckets, *J. Hydraul. Eng.*, *111*(2), 220–235.
Mulder, T., J. P. M. Syvitski, S. Migeon, J. C. Faugeres, and B. Savoye (2003), Marine hyperpycnal flows: Initiation, behavior and related deposits, *Mar. Pet. Geol.*, *20*, 861–882.
Muto, T. (2001), Shoreline autoretreat substantiated in flume experiments, *J. Sediment. Res.*, *71*(2), 246–254.
Nash, J. D., L. F. Kilcher, and J. N. Moum (2009), Structure and composition of a strongly stratified, tidally pulsed river plume, *J. Geophys. Res.*, *114*, C00B12, doi:10.1029/2008JC005036.
Nittrouer, C. A. (1999), STRATAFORM: Overview of its design and synthesis of its results, *Mar. Geol.*, *154*, 3–12.
Nittrouer, C. A., and L. D. Wright (1994), Transport of particles across continental shelves, *Rev. Geophys.*, *32*, 85–113, doi:10.1029/93RG02603.
Nittrouer, J. A., D. Mohrig, M. A. Allison, and A. P. B. Peyret (2011), The Lowermost Mississippi River: A mixed bedrock-alluvial channel, *Sedimentology*, *58*, 1914—1934, doi:10.1111/j.1365-3091.2011.01245.x.
Nittrouer, J. A., J. Shaw, M. P. Lamb, and D. Mohrig (2012), Spatial and temporal trends for water-flow velocity and bed-material sediment transport in the lower Mississippi River, *Geol. Soc. Am. Bull.*, *124*, 400–414, doi:10.1130/B30497.1.
Opreanu, G. (2010), Identifying erosion areas along the Danube on the basis of grain-size and hydrologic parameters, *Geo-Eco-Marina*, *16*, 101–106.
Paola, C. (2000), Sedimentology and sedimentary basins: From turbulence to tectonics, *Nature*, *405*(6783), 123–123.
Paola, C., G. Parker, R. Seal, S. K. Sinha, J. B. Southard, and P. R. Wilcock (1992), Downstream fining by selective deposition in a laboratory flume, *Science*, *258*(5089), 1757–1760.
Paola, C., R. R. Twilley, D. A. Edmonds, W. Kim, D. Mohrig, G. Parker, E. Viparelli, and V. R. Voller (2011), Natural processes in delta restoration: Application to the Mississippi Delta, *Annu. Rev. Mar. Sci.*, *3*, 67–91, doi:10.1146/annurev-marine-120709-142856.
Parker, G. (2004), 1-D sediment transport morphodynamics with applications to rivers and turbidity currents, e-book. [Available at http://vtchl.uiuc.edu/people/parkerg/morphodynamics_e-book.htm.]
Parker, G., and O. Sequeiros (2006), Large scale river morphodynamics: Application to the Mississippi Delta, River flow 2006 Conference, Lisbon, Portugal, in *Proceedings of International Conference on Fluvial Hydraulics*, edited by R. M. L. Ferreira et al., pp. 3–11, Taylor and Francis, London.
Parker, G., T. Muto, Y. Akamatsu, W. E. Dietrich, and J. W. Lauer (2008a), Unravelling the conundrum of river response to rising sea-level from laboratory to field. Part I: Laboratory experiments, *Sedimentology*, *55*(6), 1643–1655, doi:10.1111/j.1365-3091.2008.00961.x.
Parker, G., T. Muto, Y. Akamatsu, W. E. Dietrich, and J. W. Lauer (2008b), Unravelling the conundrum of river response to rising sea-level from laboratory to field. Part II. The Fly-Strickland River system, Papua New Guinea, *Sedimentology*, *55*, 1657–1686.
Powell, E. J., W. Kim, and T. Muto (2012), Varying discharge controls on timescales of autogenic storage and release processes in fluvio-deltaic environments: Tank experiments, *J. Geophys. Res.*, *117*, F02011, doi:10.1029/2011JF002097.
Rajaratnam, N. (1976), *Turbulent Jets*, 302 pp., Elsevier, New York.
Rajaratnam, N. (1981), Erosion by turbulent jets, *J. Hydraul. Res.*, *19*(4), 339–358.
Rajaratnam, N., and B. Berry (1977), Erosion by circular turbulent wall jets, *J. Hydraul. Res.*, *15*(3), 277–289.
Rajaratnam, N., and R. K. Macdougall (1983), Erosion by plane wall jets with minimum tailwater, *J. Hydraul. Eng.*, *109*(7), 1061–1064.
Rowland, J. C., M. T. Stacey, and W. E. Dietrich (2009), Turbulent characteristics of a shallow wall-bounded plane jet: Experimental implications for river mouth hydrodynamics, *J. Fluid Mech.*, *627*, 423–449, doi:10.1017/S0022112009006107.

Rowland, J. C., W. E. Dietrich, and M. T. Stacey (2010), Morphodynamics of subaqueous levee formation: Insights into river mouth morphologies arising from experiments, *J. Geophys. Res.*, *115*, F04007, doi:10.1029/2010JF001684.

Saad, M. B. A. (2002), Nile River morphology changes due to the construction of high Aswan dam in Egypt, Ministry of Water Resources and Irrigation Report, Egypt, 14 pp.

Schiller, R. V., and V. H. Kourafalou (2010), Modeling river plume dynamics with the HYbrid Coordinate Ocean Model, *Ocean Modell.*, *33*(1–2), 101–117.

Shaw, J. B., and D. Mohrig (2013), The importance of erosion in distributary channel network growth, Wax Lake Delta, Louisiana, USA, *Geology*, *42*(1), 31–34, doi:10.1130/G34751.1.

Shaw, J. B., D. Mohrig, and S. K. Whitman (2013), The morphology and evolution of channels on the Wax Lake Delta, Louisiana, USA, *J. Geophys. Res. Earth Surf.*, *118*, 1562–1584, doi:10.1002/jgrf.20123.

Sheets, B. A., T. A. Hickson, and C. Paola (2002), Assembling the stratigraphic record: Depositional patterns and time-scales in an experimental alluvial basin, *Basin Res.*, *14*, 287–301.

Shinneeb, A. M., R. Balachandar, and J. D. Bugg (2010), Confinement effects in shallow-water jets, *J. Hydraul. Eng.*, *137*(3), 300–314, doi:10.1061/(ASCE)HY.1943-7900.0000306.

Slingerland, R., J. W. Harbaugh, and K. Furlong (1994), *Simulating Clastic Sedimentary Basins: Englewood Cliffs*, Prentice Hall, New Jersey.

Snow, R. S., and S. L. Slingerland (1987), Mathmatical modeling of graded river profiles, *J. Geol.*, *95*, 15–33.

Sui, J., M. A. A. Faruque, and R. Balachandar (2008), Influence of channel width and tailwater depth on local scour caused by square jets, *J. Hydro-environ. Res.*, *2*(1), 39–45.

Swenson, J. B., and T. Muto (2007), Response of coastal plain rivers to falling relative sea-level: Allogenic controls on the aggradational phase, *Sedimentology*, *54*, 207–221.

Swenson, J. B., C. Paola, L. Pratson, V. R. Voller, and A. B. Murray (2005), Fluvial and marine controls on combined subaerial and subaqueous delta progradation: Morphodynamic modeling of compound-clinoform development, *J. Geophys. Res.*, *110*, F02013, doi:10.1029/2004JF000265.

Syvitski, J. P. M. (2005), The morphodynamics of deltas and their distributary channels, in *River, Coastal and Estuarine Morphodynamics*, Taylor and Francis, London, 13–25.

Syvitski, J. P. M., et al. (2009), Sinking deltas due to human activities, *Nat. Geosci.*, *2*, 681–686, doi:10.1038/ngeo629.

Tornqvist, T. E., C. Paola, G. Parker, K. Liu, D. Mohrig, J. M. Holbrook, and R. R. Twilley (2007), Comment on “Wetland sedimentation from Hurricanes Katrina and Rita”, *Science*, *316*, doi:10.1126/science.1136780.

Wong, M., and G. Parker (2006), Reanalysis and Correction of Bed-Load Relation of Meyer-Peter and Müller Using Their Own Database, *J. Hydraul. Eng.*, *132*(11), 1159–1168.

Wright, L. D. (1977), Sediment transport and deposition at river mouths: A synthesis, *Geol. Soc. Am. Bull.*, *88*(6), 857–868.

Wright, L. D., and J. M. Coleman (1971), Effluent expansion and interfacial mixing in the presence of a salt wedge, Mississippi River delta, *J. Geophys. Res.*, *76*(36), 8649–8661, doi:10.1029/JC076i036p08649.

Wright, L. D., and J. M. Coleman (1974), Mississippi River mouth processes: Effluent dynamics and morphologic development, *J. Geol.*, *82*, 751–778.

Wright, L. D., W. J. Wiseman, Z. S. Yang, B. D. Bornhold, G. H. Keller, D. B. Prior, and J. N. Suhayda (1990), processes of marine dispersal and deposition of suspended silts off the modern mouth of the Huanghe (Yellow River), *Cont. Shelf Res.*, *10*, 1–40.